The Journal of Immunology

HIV-1 gp120−CD4-Induced Antibody Complex Elicits CD4 Binding Site−Specific Antibody Response in Mice

Andrey Galkin, Yajing Chen, Javier Guenaga, Sijy O'Dell, Roderico Acevedo, James J. Steinhardt, Yimeng Wang, Richard Wilson, Chi-I Chiang, Nicole Doria-Rose, Alexander V. Grishaev, John R. Mascola and Yuxing Li

Supplementary Material	http://www.jimmunol.org/content/suppl/2020/02/14/jimmunol.1901051.DCSupplemental
References	This article **cites 82 articles**, 34 of which you can access for free at: http://www.jimmunol.org/content/204/6/1543.full#ref-list-1

Why *The JI*? Submit online.

- **Rapid Reviews! 30 days*** from submission to initial decision

- **No Triage!** Every submission reviewed by practicing scientists

- **Fast Publication!** 4 weeks from acceptance to publication

*average

Subscription	Information about subscribing to *The Journal of Immunology* is online at: http://jimmunol.org/subscription
Permissions	Submit copyright permission requests at: http://www.aai.org/About/Publications/JI/copyright.html
Email Alerts	Receive free email-alerts when new articles cite this article. Sign up at: http://jimmunol.org/alerts

HIV-1 gp120–CD4-Induced Antibody Complex Elicits CD4 Binding Site–Specific Antibody Response in Mice

Andrey Galkin,*,†,‡ Yajing Chen,§,1 Javier Guenaga,¶ Sijy O'Dell,‖ Roderico Acevedo,* James J. Steinhardt,*,2 Yimeng Wang,* Richard Wilson,¶ Chi-I Chiang,* Nicole Doria-Rose,‖ Alexander V. Grishaev,*,# John R. Mascola,‖ and Yuxing Li*,†,‡

Elicitation of broadly neutralizing Ab (bNAb) responses toward the conserved HIV-1 envelope (Env) CD4 binding site (CD4bs) by vaccination is an important goal for vaccine development and yet to be achieved. The outcome of previous immunogenicity studies suggests that the limited accessibility of the CD4bs and the presence of predominant nonneutralizing determinants (nND) on Env may impede the elicitation of bNAbs and their precursors by vaccination. In this study, we designed a panel of novel immunogens that 1) preferentially expose the CD4bs by selective elimination of glycosylation sites flanking the CD4bs, and 2) minimize the nND immune response by engineering fusion proteins consisting of gp120 Core and one or two CD4-induced (CD4i) mAbs for masking nND epitopes, referred to as gp120–CD4i fusion proteins. As expected, the fusion proteins possess improved antigenicity with retained affinity for VRC01-class, CD4bs-directed bNAbs and dampened affinity for nonneutralizing Abs. We immunized C57BL/6 mice with these fusion proteins and found that overall the fusion proteins elicit more focused CD4bs Ab response than prototypical gp120 Core by serological analysis. Consistently, we found that mice immunized with selected gp120–CD4i fusion proteins have higher frequencies of germinal center–activated B cells and CD4bs-directed memory B cells than those inoculated with parental immunogens. We isolated three mAbs from mice immunized with selected gp120–CD4i fusion proteins and found that their footprints on Env are similar to VRC01-class bNAbs. Thus, using gp120–CD4i fusion proteins with selective glycan deletion as immunogens could focus Ab response toward CD4bs epitope. *The Journal of Immunology*, 2020, 204: 1543–1561.

The HIV-1 envelope glycoprotein spike (Env) is a trimer of heterodimers, with each heterodimer consisting of gp120 and gp41 subunits. Env is the sole viral protein on the surface of the virus particle, which mediates virus entry initiated by the high-affinity interaction between the CD4 primary receptor and the cognate CD4 receptor binding site (CD4bs) on gp120 subunit (1). Subsequent Env conformational rearrangement triggered by this contact results in the formation of the chemokine coreceptor binding site on gp120, which eventually leads to cell–viral membrane fusion and virus entry (2). Because of its key biological function, CD4bs is one of the most conserved epitopes targeted by neutralizing Abs (NAbs) on the surface of the virus (3, 4). Potent and broadly neutralizing CD4bs-directed Ab responses are observed during the chronic stage of infection, although at relatively low frequency (5–9). Many CD4bs-directed broadly neutralizing Abs (bNAbs) have been isolated during the last few years aided by the advancement of single B cell sorting and cloning technology (10–14), including the prototypic CD4bs bNAb VRC01, which neutralizes >90% of circulating HIV-1 viruses and binds Env in a mode mimicking the receptor CD4 (10, 11, 13, 15, 16). CD4bs, as the supersite of virus vulnerability, is thereby an attractive target for development of HIV-1 vaccine.

*Institute for Bioscience and Biotechnology Research, University of Maryland, Rockville, MD 20850; †Department of Microbiology and Immunology, University of Maryland School of Medicine, Baltimore, MD 21201; ‡Center of Biomolecular Therapeutics, University of Maryland School of Medicine, Baltimore, MD 21201; §Department of Immunology and Microbiology, Scripps Research, La Jolla, CA 92037; ¶International AIDS Vaccine Initiative Neutralizing Antibody Center at Scripps Research, La Jolla, CA 92037; ‖Vaccine Research Center, National Institute of Allergy and Infectious Diseases, National Institutes of Health, Bethesda, MD 20892; and #National Institute of Standards and Technology, Gaithersburg, MD 20899

1Current address: Sorrento Therapeutics, San Diego, CA.

2Current address: AstraZeneca, Gaithersburg, MD.

ORCIDs: 0000-0003-3912-7482 (J.G.); 0000-0001-9534-716X (R.A.); 0000-0002-7718-5344 (R.W.); 0000-0002-5293-4695 (J.R.M.).

The elicitation of CD4bs bNAbs by vaccination, however, is a challenging task yet to be accomplished. The Env-based, native-like trimer immunogens, such as the SOSIP.664 trimer (17), have been shown to elicit little CD4bs bNAb response so far (18–20). The results of multiple immunogenicity studies suggest that limited accessibility of the CD4bs and the presence of undesirable immunodominant determinants on the Env immunogens may impede the elicitation of bNAbs and/or their precursors by vaccination (18–26). The periphery of Env CD4bs is shielded by surrounding *N*-glycans, which restricts Ab access but allows CD4 receptor engagement to initiate viral entry (27). VRC01-class CD4bs bNAbs, of which Ig genes carry sufficient somatic hypermutations (SHM), are able to approach the CD4bs on the viral Env functional spike without clashing with the *N*-glycans surrounding the CD4bs. However, the naive VRC01-class germline precursors display weak or no apparent affinity for most Envs (28, 29), suggesting that poor initial activation of CD4bs bNAb precursors by Env immunogens may account for the failure of bNAb-response elicitation. In addition, the frequencies of B cell precursors for CD4bs bNAbs are relatively low (30, 31) in the human B cell repertoires, whereas their competitors, the nonbroad CD4bs precursors often with relatively high frequencies, could readily outcompete them for activation in the germinal center (GC) where the precursors encounter Env Ags and Th cells (32). Our previous work collectively suggest that trimeric Env vaccine elicits CD4bs-directed Abs but of limited breadth because of imprecise and inefficient targeting of this region (22, 24, 33), similar to the observation of frequent occurrence of non-bNAb response in natural infections.

Extensive structural and functional analysis of VRC01-class bNAbs revealed that they partially mimic CD4 receptor and approach the Env spike at a more favorable angle than other CD4bs non-NAbs (non-bNAbs) (11, 34–36). In contrast, the footprints of prototypic CD4bs non-bNAbs isolated from HIV-1–infected individuals, such as F105 or nonhuman primates (NHP) immunized with experimental vaccine candidate, are similar and only partially overlap with those of VRC01 (24, 25, 33). The CD4bs non-bNAbs have substantial contact with two Env immunodominant elements: the bridging sheet area (coreceptor binding site) and the inner domain of Env (24, 33, 37), which are inaccessible in the Env-native functional trimer but well exposed in the monomeric gp120 or Env trimers, adopting a more open configuration. To direct Ab response away from the bridging sheet, in previous work, we used CD4-induced (CD4i) Ab 17b to form complex with gp120 Core, followed by stabilization with chemical cross-linking as immunogen (38). The binding of 17b to Env bridging sheets area would result in the blockage of this unfavored immunodominant epitope and, thus, refocus the immune response to the CD4bs epitope (38). Rabbits immunized with the gp120–17b complex generated Abs with footprints on gp120 more distal from the bridging sheet than CD4bs non-bNAbs, including F105 and CD4bs mAbs isolated from NHP animals immunized by YU2gp140-F trimer. This study suggested that the gp120–CD4i complex could be an effective priming immunogen to redirect immune response away from undesired immunodominant regions, particularly the bridging sheets region, and shift focus to bNAb epitopes.

In the present work, to extend our finding in exploiting gp120–CD4i mAb complex as immunogen for immune focusing, we designed a panel of immunogens to increase the exposure of CD4bs epitope and to conceal the nonneutralizing epitope clusters, such as the bridging sheet and inner domain. We selected a variable-loop, V1-V3–deleted gp120 Core with well-defined structure, namely YU2 gp120 Core V3S (gp120 Core) (39), as prototype immunogen to perform further modifications. We then selectively removed two of the CD4bs-flanking *N*-glycans from the gp120 Core, as suggested by previous studies (28, 29), to increase the CD4bs exposure, which resulted in a modified gp120 Core lacking *N*-glycans on residues 276 and 463 (CoreD). Subsequently, we created CoreD-derived immunogens consisting of CoreD fused with functional moieties of one or two CD4i mAbs, including 17b, the CD4i mAb recognizing the bridging sheet, and A32, a member of a different class of CD4i mAbs, which bind the inner domain of Env (40, 41) to conceal the corresponding nonneutralizing epitopes. We demonstrated that the CD4i fusion proteins retained desirable affinity for VRC01-class Abs. Moreover, we immunized mice with the CD4i fusion proteins and found that the sera of these mice had Ab response more focused on CD4bs than the mice immunized with gp120 Core alone. Furthermore, we isolated CD4bs-directed mAbs from the mice immunized with gp120–CD4i fusion protein immunogen, which had footprints on Env similar to those of VRC01-class Abs. Our study suggested that immunization with gp120–CD4i fusion proteins with CD4bs-flanking glycan deletions and masking predominant nonneutralizing epitopes could be used to prime focused Ab response toward the CD4bs epitope for eliciting bNAb response.

Materials and Methods

Modeling of CD4i fusion proteins

YU2 gp120 Core (Protein Data Bank [PDB]: 3TGQ) was a base structure to model CD4i fusion proteins (42). The ClusPro server 2.0 (43) was used in the Ab mode to produce structural models of the core in complex with A32 (PDB: 3TNM) (44). The position of the 17b was derived from x-ray structure of the YU2 gp120 in complex with 17b (PDB: 1G9N) (3). The structure of Vc813 and mouse mAbs were modeled by Rosetta3 (45). Mouse mAb in complexes with gp120 Core were modeled using local docking protocol (Rosetta3) on Rosie server (http://rosie.graylab.jhu.edu/docking2). UCSF Chimera (46) and Modella 9.14 (47) were used for structure manipulation, visualization, and analysis.

Preparation of proteins

All CD4i fusion constructs were codon optimized and cloned into pcDNA3.1(–) using EcoRI and HindIII (GenScript, Piscataway, NJ). The proteins were expressed by transient transfection in 293F cells. Supernatants were harvested 5 d posttransfection, filtered, and purified by cOmplete His-Tag Purification Resin (Roche, Basel, Switzerland). The RSC3 core (11), BG505.SOSIP.664 trimer (48), with their CD4bs knockout (KO) variants, and 16055 NFL TD CC ΔGly4 bearing 4 glycan deletions (residues 276, 301, 360, and 463) (49) were purified as described previously.

To remove aggregates and undesired oligomeric states, all protein samples were subject to size exclusion chromatography (SEC) on Superpose 6 10/300 GL or Superdex 200 columns (GE Healthcare) pre-equilibrated with PBS in an ÄKTA pure station. Protein sample purity was analyzed by SDS-PAGE.

Mouse immunization and blood/tissue collection

All procedures were carried out by following animal research guidelines and approved by Institutional Animal Care and Use Committee. The female C57BL/6 mice (age 6–10 wk) were vaccinated three times via i.m. injection in two sites (hamstring muscle in each leg) on weeks 0, 4, and 8 (Fig. 4B). Each animal received a 10 μg dose of protein immunogen in 100 μl of PBS containing 5 μl of Adjuplex (Advanced BioAdjuvants) as adjuvant. For serum preparation, the blood samples were collected retroorbitally on weeks 0, 2, and 6. The terminal bleeds and tissue harvest were performed on week 11. To prepare cell suspensions for flow cytometry, lymphocytes were released from lymph nodes or spleens by mincing the tissues into ~2-mm pieces with scalpels in RPMI 1640 medium, followed by passing through a cell strainer. Cells from spleens were further purified by density gradient centrifugation with Ficoll-Paque PLUS (GE Healthcare). After washing with PBS, cells were resuspended in BAM-BANKER (Wako Chemicals) and frozen gradually to −80˚C, followed by storage in liquid nitrogen prior to the staining and sorting experiments.

Flow cytometry and Ag-specific B cell sorting

Cryopreserved mouse lymphocytes were thawed quickly in 37˚C water bath and treated with DNase I (10,000 U/ml; Roche) in RPMI 1640 with 10%

FBS and stained with Aqua Dead Cell Staining (Life Technologies), followed by a mixture of Abs for identifying B cells essentially as described previously with minor modifications (50, 51). Briefly, a mixture of Abs diluted in RPMI 1640/10% FBS, which contains CD3 (clone 17A2), F4/80 (clone BM8), Gr1 (clone RB6-8C5) (PerCp/Cy5.5; BioLegend), GL7 (clone GL7) (FITC; BD Pharmingen), CD19 (clone 1D3) (APC-Cy7; BD Pharmingen), B220 (clone RA3-6B2) (Alexa Fluor 700; BioLegend), IgD (clone RA3-6B2) (Pacific Blue; BioLegend), IgM (clone R6-60.2) (PE/Cy7; BD Pharmingen), CD38 (clone 90) (BV605; BD Biosciences), and Fas (clone Jo2) (BV750; BD Biosciences), was used to stain the cells.

To illustrate CD4bs-specific B cell, CoreD–n5i5–17b and the CD4bs KO mutant D368R/D474A carrying an AviTag at the C terminus were biotinylated with BirA-500 biotin ligase (AviTag Technology; Avidity, Aurora, CO). Before adding to the Ab mixture, wild-type (WT) CoreD–n5i5–17b was conjugated with streptavidin–allophycocyanin (Life Technologies), and the CD4bs KO mutant was conjugated with streptavidin–PE (Life Technologies) as described previously (52). CD4bs-specific B cells were identified as CD19+B220+CD3−Gr1−F4/80−IgD−, followed by binding phenotype to CD4bs-specific Ag probe pair (CoreD–n5i5–17b WT+ CD4bs KO−). GC B cells are initially gated as CD19+B220+CD3−Gr1−F4/80−IgD−, followed by GC-specific markers GL7+Fas+. Memory B cells are gated as CD19+B220+CD3−Gr1−F4/80−IgD−CD38+. CD4bs-directed memory B cells are subsequently gated by CD4bs-specific Ag probe pair (CoreD–n5i5–17b WT+ CD4bs KO−) binding phenotype.

To sort CD4bs-specific, class-switched B cells for Ig gene amplification, we gated class-switched B cells as CD19+B220+CD3−Gr1−F4/80−IgD−IgM−, followed by CoreD–n5i5–17b WT+CD4bs KO−–binding phenotype. These cells were then sorted at single-cell density into 96-well plates using BD FACSAria III cell sorter (BD Biosciences).

mAb cloning and production

The sorted CD4bs-specific, class-switched B cells were subjected to single-cell reverse transcription and PCR reactions to amplify Ig sequences as previously described (11, 52, 53). The single-cell, RT-PCR–generated Ab V(D)J gene segments were analyzed by ImMunoGeneTics (IMGT)/HighV-QUEST using mouse Ig germline reference database (54). The variable domains of H and L chains were cloned into corresponding IgG expression vectors, described previously (52, 53) to generate mouse-human chimeric Abs with mouse Ig variable regions and human IgG1 constant regions. The culture supernatant of 293F cells, cotransfected with the IgG expression vectors, was used to purify mouse mAbs on Protein A Sepharose Columns (GE Healthcare). For Ab Fab fragment production, the H chain variable domain was cloned into Fab expression vector described previously (55). Fab fragments were expressed in 293F cells and purified by cOmplete His-Tag Purification Resin (Roche).

Human and NHP Abs

The HIV-specific human mAb F105 was provided by M. Posner (Dana–Farber Cancer Institute), and PGV04 were provided by D. Burton (Scripps Research). VRC01, VRC03, VRC06, and germline version of bNAb VRC01 (VRC01GL) were previously described (11, 24, 28, 35). NHP CD4bs mAbs GE136 and GE148 were previously described (24, 55). The CD4Ig plasmid expression construct was provided by J. Sodroski (Dana–Farber Cancer Institute). The CD4i mAb 17b was provided by J. Robinson (Tulane University).

ELISA

The initial antigenic profiles of CD4i fusion proteins and the specificities of mouse mAb were obtained by ELISAs, as described previously (38, 52). Briefly, for CD4i fusion protein binding, anti–His Tag Ab (R&D Systems) was coated onto MaxiSorp plates (Nunc; Thermo Fisher Scientific) at 2 μg/ml in PBS overnight at 4°C. After blocking with 2% dry milk and 5% FBS, CD4i fusion proteins were added to each well at 2 μg/ml for 30 min at room temperature, followed by the addition of the immune sera, human or mouse mAbs, respectively, in 5-fold serial dilutions in blocking buffer starting at 1:100 dilution for sera and 10 μg/ml for mAbs. After incubation with goat anti-mouse or anti-human IgG-HRP conjugate (Jackson ImmunoResearch Laboratories, West Grove, PA), the signal was developed with tetramethylbenzidine substrate (Life Technologies).

Competition ELISA was performed as previously described (11). Briefly, CoreD–n5i5–17b was captured in the wells precoated with anti–His Tag Ab (R&D Systems). The unlabeled competitors, mouse mAbs, were diluted in blocking buffer and added in 5-fold serial dilutions, starting at 50 μg/ml. After 30-min incubation at 37°C, biotin-labeled VRC01 or CD4Ig at a single concentration was added to the wells. This concentration was determined by previous titration experiments to give an OD 450-nm

value in the range of 1–2. Biotin-labeled protein binding was detected by secondary streptavidin−HRP polymer (Sigma-Aldrich) at 1:5000 dilutions in blocking buffer (10× diluted with PBS containing 0.05% Tween 20). Between each incubation step, the plates were washed four times with PBS containing 0.05% Tween 20. The HRP-conjugate signal was developed by the addition of 100 μl of tetramethylbenzidine single solution (Invitrogen, Camarillo, CA) to each well. The reaction was stopped by adding 100 μl of 3% sulfuric acid, and optical absorbance was measured at 450 nm.

Ab binding kinetics

The Ab binding kinetics was performed by biolayer light interferometry (BLI) using an Octet RED96 instrument (ForteBio; Pall Life Sciences) as previously described (24). In brief, mAbs at 10 μg/ml in PBS/0.2% Tween 20/0.01% BSA were captured on the surface of the anti-human IgG Fc biosensors (ForteBio). The biosensor tip was then immersed in wells containing protein samples with different concentrations. ForteBio Data Analysis 8.2 software was used for data processing and global fitting.

HIV-1–neutralization assays

The mouse sera and IgG-neutralization assays were performed with Env-pseudoviruses and TZM-bl target cells, as described previously (56–58). Mini panel of five pseudoviruses was used: BG505.W6M.C2. T332N, MW965.26, 45_01dG5, MN.3, and HXBc2.DG (Supplemental Fig. 4). The background neutralization was assessed with non-HIV pseudovirus SIVmac251.30.SG3. Serum ID_{50} titer, the reciprocal dilution factor of serum sample achieving IC_{50} of virus entry was determined by using a five-parameter hill slope equation fitting as previously described (58). The mouse sera samples with high-background neutralization against SIV pseudovirus (ID_{50} above 50) were excluded from virus neutralization analysis, which included one from naive animal group, one from A32–CoreD–Vc813-immunized group, and three from A32–CoreD–17b-immunized group. However, serum/tissue samples from animals with such serum virus–neutralization background, caused likely by serum cytotoxicity to infection target cells, is irrelevant to other Ab and B cell response analysis (ELISA binding and B cell FACS) in our study. Therefore, we did not exclude these serum/tissue samples with serum virus neutralization background from ELISA binding assays and FACS analysis.

Small-angle x-ray scattering

Complexes of CoreD–n5i5–17b with VRC01 and 1D3 Fabs were prepared by mixing purified monomeric CoreD–n5i5–17b with excess quantities of Fabs and incubated overnight at 4°C. The complexes were isolated by SEC on Superpose 6 10/300 GL (GE Healthcare). Solution x-ray scattering data were collected for samples containing between 2.0 and 0.5 mg/ml of protein complex to investigate the effect of sample concentration on the scattering data. Small-angle x-ray scattering (SAXS) data collections were performed on a laboratory-based instrument (Institute for Bioscience and Biotechnology Research, Rockville, MD), all carried out at 25°C. SAXS data were collected using 8-keV incident radiation from a Rigaku 007HF rotating anode source and a PILATUS 300K detector with programmable positioning covering the Q-range from 0.008 to 0.8 Å^{-1}. Two-dimensional scattering data were processed using instrument-specific routines correcting for the sample transmission, detector pixel sensitivity, and solid angle per pixel while using dynamic masking to remove the data impacted by stray cosmic radiation. Buffer scattering was subtracted from sample curves using protein concentration-based solvent volume fractions.

The experimental x-ray scattering data were authenticated by good agreement between 1) the radii of gyration ($R_{gyr}^{Guinier}$) extracted from the lowest-angle data and those obtained by the Fourier transforms of the complete scattering curves (R_{gyr}^{GNOM}) as indicator of monospersity; 2) the molecular masses of the scattering complex particles extracted from SAXS data (MW^{SAXS}) and the expected molecular mass ($MW^{Expected}$) as indicator of monomeric status; and 3) the extracted maximum dimensions (D_{max}^{GNOM}) of the scattering complex particles and the corresponding all-atom models. Subsequently, two complementary approaches were taken for the structural interpretation of SAXS data.

First, all-atom models of the complexes were generated and validated. The position of the VRC01 Fab in complex with CoreD–n5i5–17b was derived from the crystal structure of VRC01 Fab: gp120 Core complex (PDB: 3ngb), with its scattering pattern predicted via FoXS software (59), which is in good agreement with the experimental SAXS data (fit parameter, χ= 1.36) (Fig. 11A, left). Furthermore, Rosetta Ab and docking protocols were used to generate coordinates of 1D3 Fab: CoreD–n5i5–17b complex. Ten top-ranking Rosetta models were selected to calculate scattering patterns by FoXS server based on the all-atom models of 1D3 Fab: CoreD–n5i5–17b complex, which were subsequently compared with

the experimental SAXS profile. The second-ranking model by Rosetta docking algorithm showed the best fit to SAXS data (χ= 1.21) (Fig. 11A, right).

In the second approach, all-atom models of the VRC01 Fab or 1D3 Fab: CoreD–n5i5–17b complex were validated by reconstructing low-resolution ab initio envelope shapes from the experimental SAXS data alone via DAMMIN program within the ATSAS 2.8 suite (60). The models of the complexes were represented at low resolution via densely packed dummy atoms (beads). Simulated annealing algorithm was used to find configurations that fit well with experimental data (61) while enforcing compact and connected shapes of the scattering particles. Ab initio DAMMIN bead models reconstructed for the complex of CoreD–n5i5–17b with VRC01 or 1D3 provided overall shape of the complex with low resolution (Fig. 11B, left and middle panels, respectively). All of the 10 DAMMIN models for the 1D3 Fab: CoreD–n5i5–17b complex generated with different initial random number seeds were in good agreement with the experimental scattering profile (χ ~0.95). These models also showed good structural convergence, as indicated by the normalized spatial discrepancy of 1.15 ± 0.08. Similarly, 10 ab initio models of VRC01 Fab: CoreD–n5i5–17b complex were in good agreement with the experimental profile (χ = 1.29), likewise exhibiting good structural convergence (normalized spatial discrepancy = 0.7 ± 0.07). The averaged and consistency-filtered DAMMIN bead models were subsequently used to calculate the overall molecular surfaces displayed in Fig. 11B.

Data processing and statistical analysis

Data processing and statistical analysis was performed with GraphPad Prism version 7. Comparison of three or more groups was conducted with one-way ANOVA. Statistical evaluation of difference between two groups was performed with t test. Statistical significance was determined as *$p < 0.05$, **$p < 0.01$, ***$p < 0.001$, and ****$p < 0.0001$.

Results

Design and production of the gp120–CD4i fusion immunogens

Previously, it was observed that the presence of certain glycans in the loop D and V5 regions of Env often leads to limited exposure of CD4bs and hampering the initiation (28, 29) and maturation (62) of VRC01-class bNAb lineages. We chose a gp120 Core variant gp120ΔV1V2(2b)V3S core (Core), which was described previously (42, 63) as the model immunogen to present CD4bs epitope. As the first step to improve the elicitation of CD4bs-directed Ab response, we constructed a variant of YU2 Core, with CD4bs epitope preferentially exposed by selective elimination of its flanking N-linked glycosylation sites. Sequence analysis and computer modeling suggest that two potential N-linked glycosylation sites of the Core, N276 in loop D, and N463 in V5 region, respectively, locate in the vicinity of CD4bs and could interfere with the binding of VRC01-class Ab precursors to the Core, particularly the VRC01GL (Fig. 1A). We replaced these residues with aspartates by mutagenesis to eliminate the corresponding potential N-linked glycosylation sites, which resulted in N276D/N463D double mutant Core variant (referred to as CoreD) (Fig. 1B), the parent of all other CD4i fusion immunogens.

Subsequently, we designed a panel of priming immunogens aimed to minimize the immune response to the nonneutralizing epitopes, including the bridging sheets and inner domain by engineering fusion proteins consisting of CoreD and one or two variable domains of CD4i mAbs to mask their cognate epitopes. We have selected three CD4i Abs: 17b (3) and Vc813 (35), which bind to the bridging sheet of gp120, and A32, which interacts with the inner domain of gp120 (44). At the time of the CD4i-fusion design, only the crystal structures of gp120 Core in complex with 17b (PDB: 1G9N and 1G9M) and unliganded A32 Fab (PDB: 3TNM) (44) were available as reference structures. Using ClusPro 2.0 docking server, we built structural model of CoreD in complex with A32 Fab. We used the model together with the crystal structure of gp120 in complex with 17b to guide the design of all CD4i fusion complexes containing A32 variable domains (Fig. 1C). To have a

common ground, gp120 Core structure was used to superimpose these structural complexes. We initially joined CoreD with single-chain variable fragment (ScFv) domains of 17b (Fig. 1D) and Vc813, respectively, to produce single CD4i-fusion group of immunogens (Fig. 1F). Subsequently, we constructed and optimized double CD4i fusion proteins based on the single CD4i fusion protein configurations (Fig. 1E, 1F, Supplemental Fig. 1) with good expression yield.

In general, the topology of the CD4i fusion proteins is determined by the spatial distance between the gp120 structural elements and the CD4i mAb variable moieties (N or C termini of the variable H chain [VH] and variable L chain [VL]) (Fig. 1C–E), which is subsequently connected by flexible peptide linkers with requisite lengths. For CoreD–A32 fusion protein, because the gp120 Core C terminus (E492^{gp120}) and the A32 VH N terminus (Q1 $^{A32\ VH}$) are proximal with a distance of 33 Å, we used a linker consisting of four tandem GGGGS (G$_4$S) units (each linker unit accounts for ~18-Å length) denoted as 4×, to connect gp120 CoreD and A32 ScFv (Fig. 1C, 1F). Of note, the distances between the gp120 Core N/C termini and 17b VH/VL vary from 76 to 61 Å, respectively. To minimize the linker length between the joining points of 17b and gp120 Core, permutated version of CoreD (CoreD PM) was used (Fig. 1D). The CoreD PM molecule has an N terminus at S199^{gp120} (Fig. 1D), encompassing residues (S199-E492)^{gp120}, followed by residues (E492-GG linker-V44) ^{gp120} and residues (V44-T123) ^{gp120} (Fig. 1D), and joining with a 4× linker [(G$_4$S)$_4$] and 17b ScFvs (64, 65) to form CoreD-17b (Fig. 1D). Subsequently, we fused A32 ScFvs to the N terminus of CoreD-17b to form double CD4i-fusion protein, A32-CoreD-17b, with a 5× linker [(G$_4$S)$_5$] (Fig. 1E, 1F).

Additionally, we used the ScFv of another CD4i mAb, Vc813 (35), to replace 17b, which resulted in single and double CD4i fusion proteins, CoreD–Vc813 and A32–CoreD–Vc813, respectively, as novel immunogen candidates (Fig. 1F). Amino acid sequences of CD4i fusion immunogens are shown in Supplemental Fig. 1. All CD4i-fusion constructs were expressed in 293F cells and purified to apparent homogeneity. SEC analysis of these fusion proteins revealed monomeric, as well as oligomeric forms, with the m.w. of the latter estimated as ~4 times that of the monomer.

The engineered immunogens display retained affinity for CD4bs bNAbs and eliminated binding to non-bNAbs

To characterize the antigenicity of these engineered Env variants, we performed ELISA and BLI assays with representative CDbs ligands. Based on the design rationale, CD4i fusion immunogens should present CD4bs bNAb epitope well with strong cognate bNAb recognition and minimized reactivity with CD4bs non-bNAbs.

We tested the binding activities of the Env variants to prototypical CD4bs bNAbs VRC01 and PGV04, respectively, by ELISA assays. In agreement with the modeling predictions, gp120 Core, CoreD (N276/N463 glycans removed), and the CD4i fusion proteins showed robust recognition with CD4bs bNAbs (Fig. 2A). In addition, consistent with the modeling, the CD4i fusion proteins demonstrated abolished binding to CD4bs non-bNAbs, including F105 derived from natural infection, and mAbs GE136/GE148, isolated from Env-immunized NHP animals (Fig. 2A). Interestingly, CoreD–A32 protein also displayed substantially diminished recognition with non-bNAbs (Fig. 2A), although no direct steric clashes were predicted between A32 ScFv moiety and these mAbs by structural analysis. Altogether, consistent with our previous studies of chemically cross-linked gp120–17b complex, CD4i fusion immunogens have attenuated binding to CD4bs non-bNAbs and generally retained affinity to bNAbs.

Next, we used BLI to obtain the detailed binding kinetics parameters for Core, CoreD, and CD4i-fusion proteins with respect to
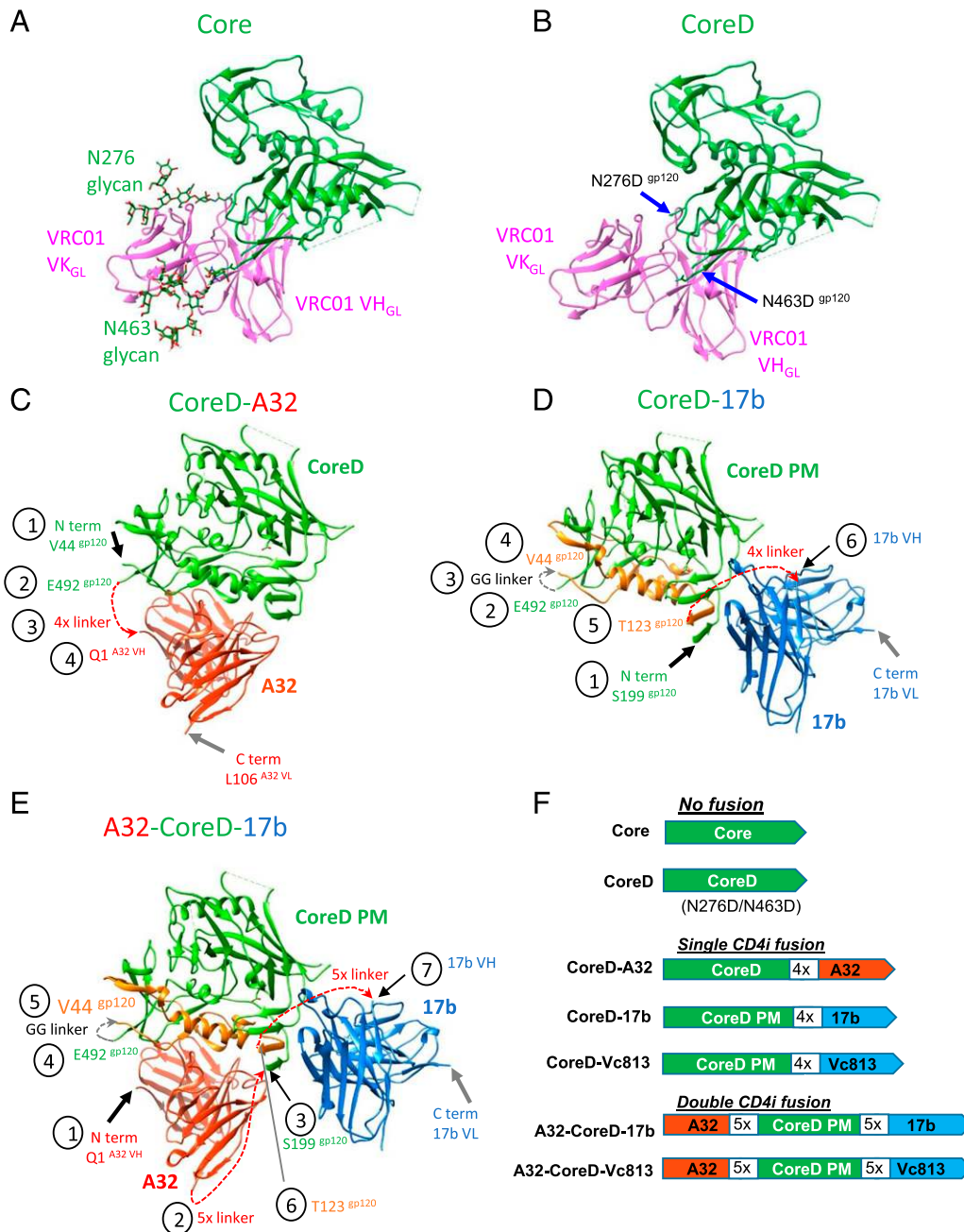
FIGURE 1. Design of the gp120–CD4i fusion proteins. (**A**) Model of YU2 gp120 Core (PDB: 3TGQ) in complex with VRC01 germline Ab (VRC01GL; PDB: 4jpk). Of note, two *N*-glycans, N276 (modeled from PDB: 5FYK) and N463 (modeled as oligomannose from http://www.glycosciences.de/), surrounding the gp120 CD4bs epitope clash with VRC01GL. (**B**) CoreD with two mutations (N276D/N463D) that remove the N276 and N463 *N*-glycans, respectively. Connectivity of gp120–CD4i fusion proteins: (**C**) CoreD–A32, CoreD (V44-E492) gp120 shown in green, and A32 in red; (**D**) CoreD-17b with circular permutation (PM): (S199-E492) gp120 shown in green, (V44-T123) gp120 in gold, and 17b in blue; (**E**) A32–CoreD–17b with circular PM: A32 in red, and the other elements are depicted as in (D). The 5× [(G4S)4] linker is depicted as red dashed line. (**F**) Linear schematic presentation of the YU2gp120 Core–based gp120–CD4i fusion protein immunogens. CoreD-PM stands for the CoreD with circular PM shown in (D) and (E). The 4× and 5× depict (G4S)4 and (G4S)5 flexible peptide linker, respectively.

the CD4bs ligands. The bNAbs VRC01, PGV04, and CD4Ig, the surrogate for the CD4 receptor, showed strong binding to all gp120 Core variants (Fig. 2B). The association rates (k_{on}; on-rate) of the Ab-Env recognition are approximately similar (Fig. 2C), whereas some difference was observed for the dissociation rates (k_{off}; off-rate), which resulted in changed affinities (K_D) (Fig. 2C). Particularly striking improvement in binding affinity was observed for VRC01; the removal of N276/N463 glycans from the Core resulted in ~40-fold decrease in K_D from 1.2 nM (Core) to 0.03 nM (CoreD). No substantial difference in affinity was observed for

PGV04 or CD4Ig binding. The overall binding affinities of the Env variants to CD4bs ligands determined by BLI were consistent with the ELISA binding data and confirmed the retained affinity for CD4bs bNAbs after removal of N276/N463 glycans and fusion with CD4i Abs, with improvement as in the case of VRC01.

Selected Env variants display augmented VRC01GL recognition

Having confirmed the ability of CD4i fusion proteins to bind strongly to mature bNAbs, we next examined the potential augmented

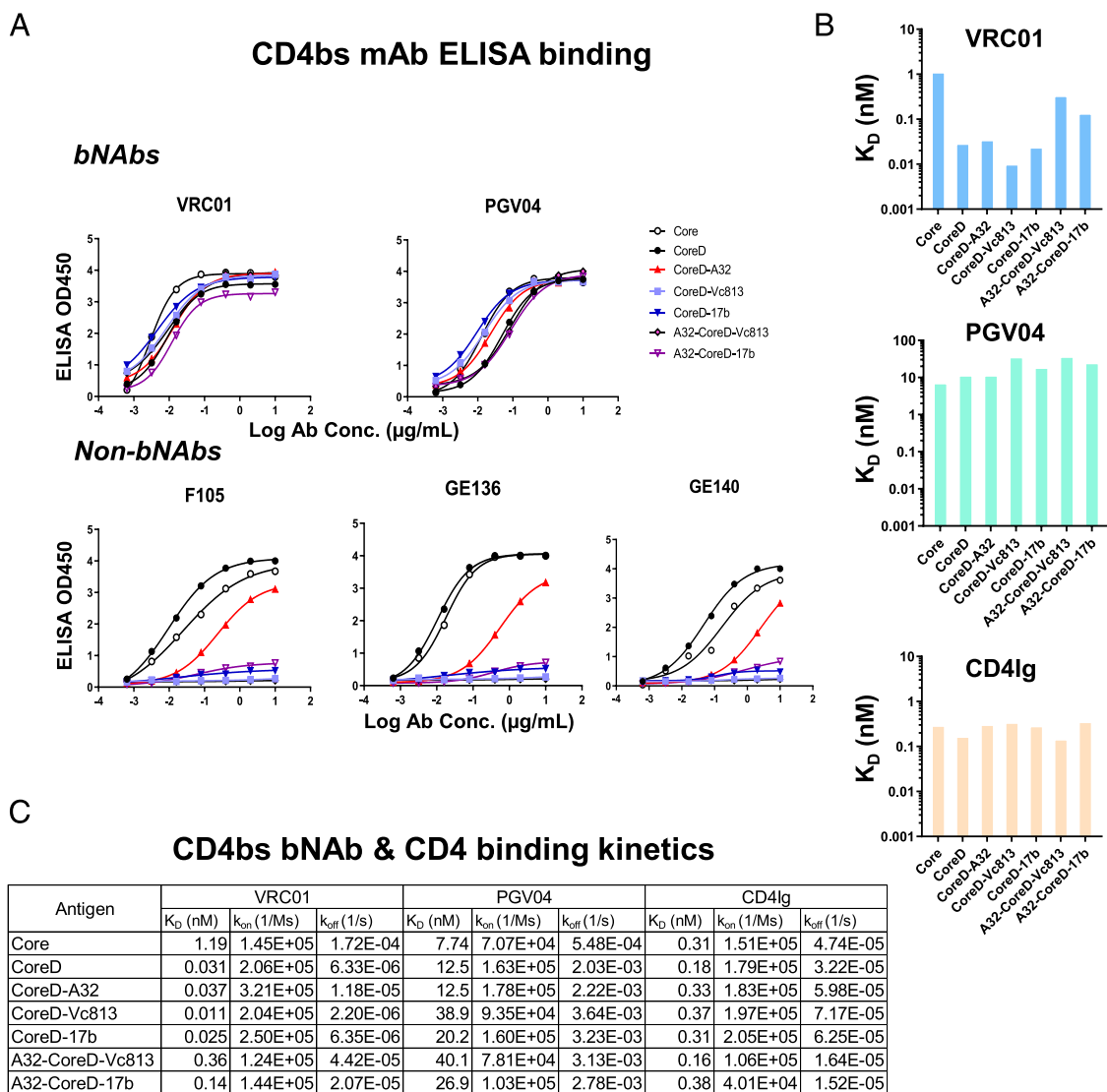FIGURE 2.   gp120–CD4i fusion proteins display retained or enhanced affinity for CD4bs bNAbs with minimized non-bNAb binding. (**A**) ELISA binding of gp120–CD4i fusion proteins to CD4bs bNAbs (VRC01 and PGV04) and non-bNAbs (F105, GE136, and GE148), in comparison with Core and CoreD. (**B**) gp120–CD4i fusion protein binding affinity (dissociation constant [K_D]) for CD4bs ligands (VRC01, PGV04, and CD4Ig) assessed by BLI. (**C**) Detailed binding kinetic analysis of gp120–CD4i fusion proteins binding to CD4bs ligands by BLI. k_{off}, dissociation rate; k_{on}, association rate; K_D, affinity or dissociation constant, calculated as k_{off}/k_{on}.

recognition of the Env variants by the naive precursor of VRC01-class bNAbs, particularly the germline-reverted VRC01 (VRC01GL) by BLI (Fig. 3). Consistent with our early observation, unmodified gp120 Core displayed no binding with VRC01GL (Fig. 3A), similar to CoreD D368A, a variant of CoreD bearing a CD4bs KO mutation D368A, which serves as negative control for the binding assay (Fig. 3A). As expected, CoreD with the elimination of two glycosylation sites of gp120 Core resulted in very weak, but detectable, binding to VRC01GL (affinity K_D = 9.5 μM, Fig. 3). Furthermore, in the cases of CoreD fused with A32, 17b, or Vc813 CD4i ScFv fragments, the binding affinities to VRC01GL are substantially improved with K_D values ranging from 59 to 100 nM (Fig. 3). Although double CD4i fusion A32–CoreD–Vc813 showed no binding to VRC01GL, A32–CoreD–17b displayed significant improvement of binding to VRC01GL (Fig. 3A). SEC of A32–CoreD–17b indicates the presence of both a monomeric form and a substantial amount of oligomer. The monomeric A32–CoreD–17b bound VRC01GL with a 204 nM affinity, whereas the oligomeric form, $_{oligo}$A32-CoreD-17b, showed an apparent affinity

of 80 nM, 2-fold higher than the monomer (Fig. 3B). Consistent with the results of previous studies (66), trimeric Env immunogens including WT BG505 SOSIP and its variant bearing a T278A mutation (glycan 276^{off}) (66), and 16055 NFL TD CC ΔGly4 bearing 4 glycan deletions (residues 276, 301, 360, and 463) (49) showed no binding to VRC01GL (Fig. 3). Therefore, our immunogen modifications led to Env variants possessing augmented VRC01GL affinity.

Immunogenicity study in mice

The immunogenicity of the various forms of CD4i-fusion proteins with favorable antigenicity was examined in C57BL/6 mice, as shown in Fig. 4. We included Core, CoreD, and five CoreD–CD4i fusion proteins as test immunogens formulated with Adjuplex as adjuvant (Fig. 4A) to compare with the prototypical Env trimer BG505 SOSIP.664, whereas mice injected with PBS/adjuvant served as a negative control group. Given the higher affinity to VRC01GL displayed by the oligomeric form A32–CoreD–17b than the monomeric form (Fig. 3), we included it as immunogen in
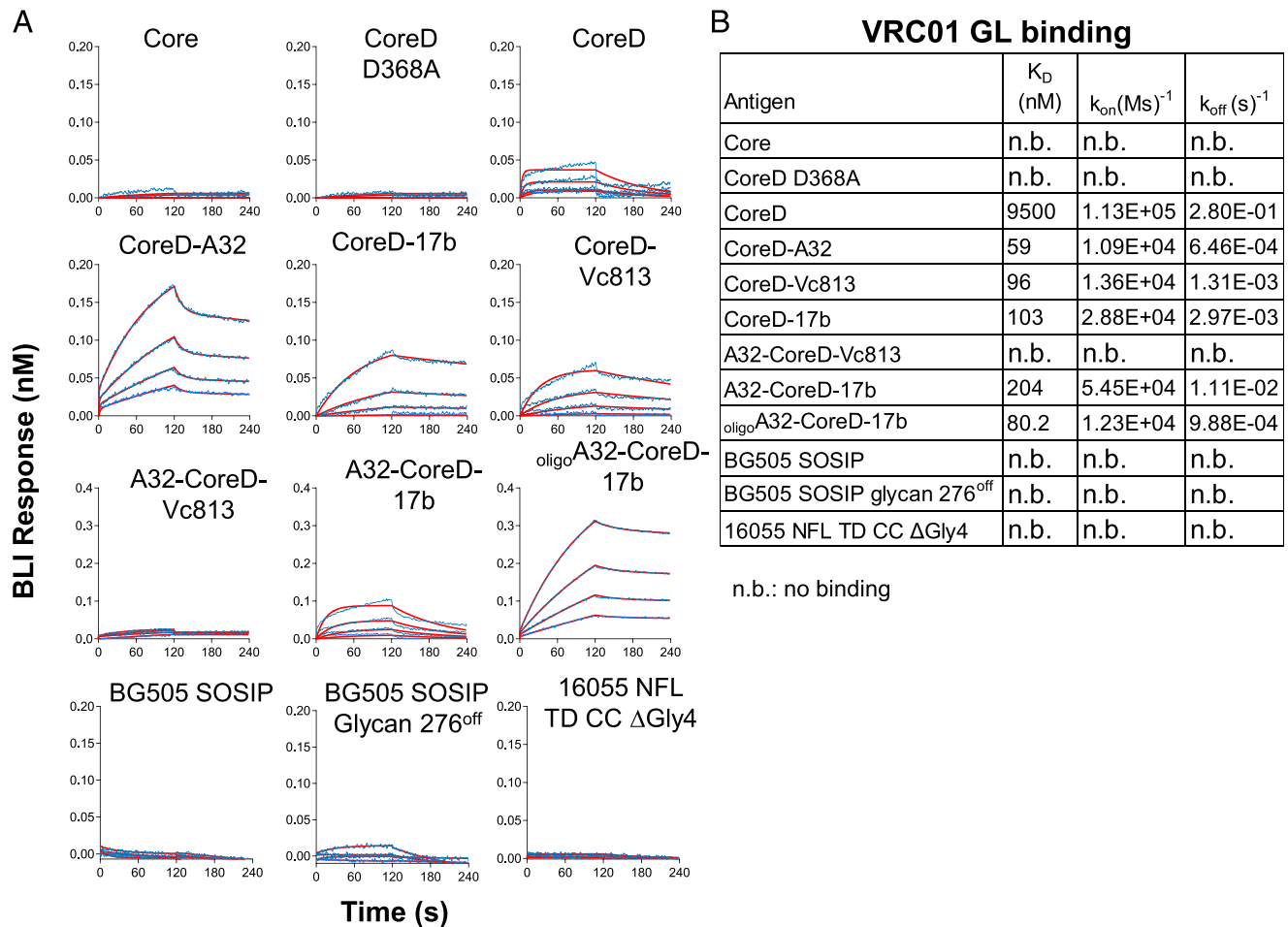
FIGURE 3. Selected gp120–CD4i fusion proteins display elevated binding affinity for VRC01 germline precursor, VRC01GL, assessed by BLI. (**A**) BLI response of gp120–CD4i fusion proteins in comparison with Core, CoreD, and trimeric Env immunogens (BG505 SOSIP variants and 16055 NFL TD CC ΔGly4). (**B**) Detailed binding kinetic analysis of gp120–CD4i fusion proteins binding to VRC01GL by BLI, in comparison with Core, CoreD, and trimeric Env immunogens. k_{on}, k_{off}, and K_D are defined as in Fig. 2C.

parallel to the monomer to examine if the oligomeric state of this CD4i fusion protein could potentially stimulate Ab response of higher quality (Fig. 4A). C57BL/6 mice (four mice per immunogen group) were inoculated with 10 μg of Env variants with Adjuplex as adjuvant on week 0. Two more injections were performed on weeks 4 and 8, respectively, to boost the response (Fig. 4B).

Novel Ag probe for analyzing CD4bs-specific Ab/B cell response

To analyze the Ab binding specificity in animal sera, we designed and produced additional gp120–CD4i fusion protein as Ag binding probe. As shown in Fig. 5A, we incorporated the ScFv of another CD4i mAb n5i5 into the CoreD–17b fusion protein to form a double CD4i fusion protein, named CoreD–n5i5–17b. n5i5 is an A32-like CD4i Ab binding to the immunodominant gp120 inner domain rich of nonneutralizing epitopes, of which crystal structure in complex with gp120 Core recently became available (67). Guided by this structure, we designed CoreD–n5i5–17b protein with a $(G_4S)_3$ linker (3×) to connect CoreD and n5i5, and a $(G_4S)_4$ linker (4×) to connect n5i5 and 17b, respectively. This newly designed fusion protein had substantially increased yield (∼0.7 mg/L) (Supplemental Fig. 2) ∼5–7 fold compared with other double CD4i fusion proteins (∼0.1 mg/L). Shortening of the length of the connecting linkers and the elimination of the parent CoreD permutation could all contribute to the overall improved

yield. Similar to A32–CoreD–17b fusion protein, CoreD–n5i5–17b strongly binds CD4bs bNAb VRC01 while displaying no binding to non-bNAbs F105 and GE136 (Fig. 5B). Furthermore, we introduced two mutations D368R/D474A to the CD4bs region of CoreD–n5i5–17b, which resulted in the CD4bs KO variant, CoreD–n5i5–17b CD4bs KO, with diminished binding to CD4bs bNAb VRC01 (∼2 logs change in binding EC_{50} value) (Fig. 5B). The combination of CoreD–n5i5–17b and its CD4bs KO variant D368R/D474A as Ag probes to analyze the mice sera would help to delineate the CD4bs-directed Ab response. Together with the BG505 SOSIP.664 native-like trimer (17) and RSC3 (resurfaced gp120 Core) (11), we set to use CoreD–n5i5–17b as a more selective Ag probe than the parental immunogen CoreD to assess the Ab responses in the mice immunized with CoreD or CoreD–CD4i fusion proteins (Fig. 5C).

Different levels of Ab response to immunodominant elements

To examine if the Ab responses elicited by CoreD–CD4i fusion proteins are different from the parental immunogen CoreD, we tested the IgG Ab binding activity of the terminal serum samples (week 11, 3 wk after the third immunization) to Ag probes including CoreD, RSC3, and BG505 SOSIP.664 trimer by ELISA. The immune serum binding activity were presented as the areas under the curves (AUC) of ELISA (Fig. 6, Supplemental Fig. 3), with binding AUC grouped into three categories of immunogens: 1) core group including Core and CoreD; 2) single CD4i-fusion
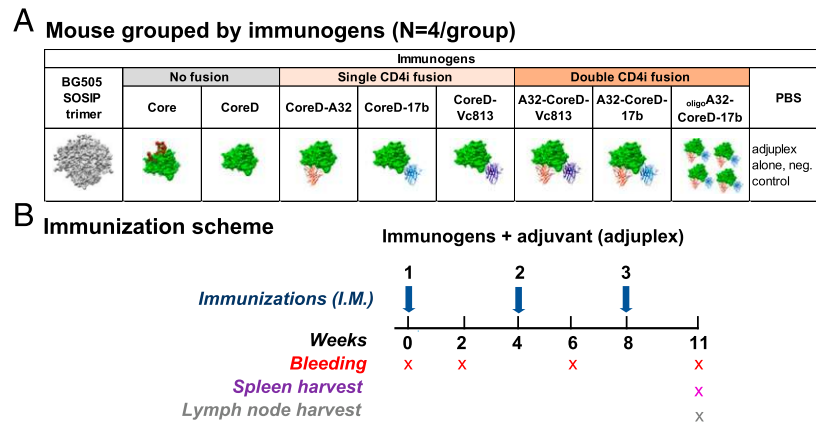
A Mouse grouped by immunogens (N=4/group)

B Immunization scheme

FIGURE 4. gp120–CD4i fusion protein immunogenicity study design. (**A**) C57BL/6 mice (*n* = 4 mice/group) were divided into 10 groups to be immunized with various immunogens formulated with adjuvant (Adjuplex) including Core, CoreD, single and double CD4i fusion proteins, with Env trimer BG505 SOSIP.664 as reference immunogen and PBS as negative control. (**B**) Immunization and sampling schedule. Mice were i.m. immunized with 10 μg of Env immunogens in Adjuplex on weeks 0, 4, and 8 (indicated by blue arrow), respectively, for a total three times. Blood sampling was performed on weeks 0 (preimmune serum), 2, 6, and 11 (2 or 3 wk after each immunization) (marked by Xs). Upon termination on week 11, the lymph nodes and spleens of the immune mice were harvested for analysis.

group including CoreD–A32, CoreD–17b and CoreD–Vc813; and 3) double CD4i-fusion group including A32–CoreD–Vc813 and A32–CoreD–17b monomer and oligomer. With CoreD as the probe, which presents the overall epitopes of gp120 Core, including the immunodominant determinants such as the inner domain and bridging sheets (Fig. 6A, Supplemental Fig. 3B), we observed that the sera from all animals immunized with CD4i-fusion proteins (single and double CD4i; Fig. 6A, left) tended to have lower CoreD binding AUC than those from the animals immunized with Core and CoreD immunogens (***$p < 0.001$). This observation is consistent with the notion that the immuno-dominant determinants, such as the inner domain and bridging sheets, are substantially masked in the CD4i-fusion proteins, which may result in attenuated elicitation of Abs to such epitopes in the CoreD Ag probe.

Next, we used the antigenically resurfaced protein core, RSC3, as Ag probe to test the animal sera. RSC3 was designed to present the structurally conserved receptor CD4 binding site specifically
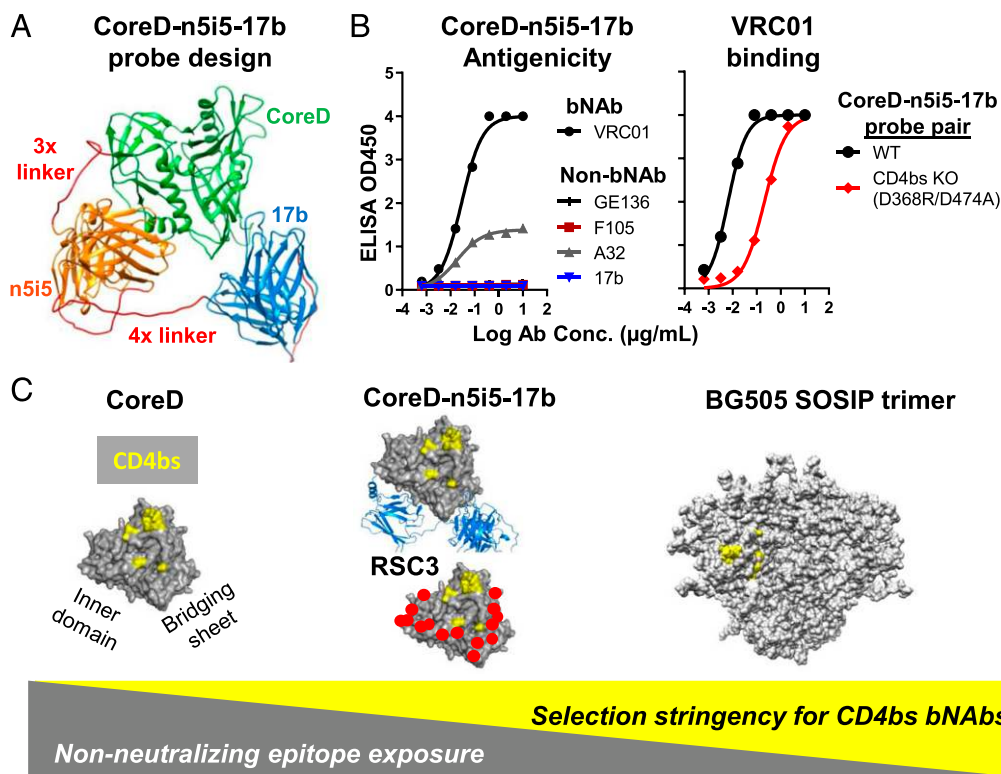
FIGURE 5. Ag probes used to investigate Ab response in mice. (**A**) The design of CoreD–n5i5–17b fusion protein as Ag probe. CoreD (green) is connected to n5i5 ScFv (gold) and 17b ScFv (blue), with 3× and 4× linkers (red) denoting three and four tandem (G₄S) flexible peptide linker modules, respectively. (**B**) ELISA binding profile of CoreD–n5i5–17b: left, it binds strongly to CD4bs bNAb VRC01 and poorly to non-bNAbs F105 and GE136, as well as CD4i mAbs, A32 and 17b; right, the CD4bs KO mutant variant (D368R/D474A) shows attenuated binding affinity for CD4bs bNAb VRC01 compared with the WT (black) Ag probe. (**C**) Schematic presentation of the surface structural models of the Env Ag probes used for profiling immune mouse serum Ab response specificity. CD4bs epitope is denoted in yellow color. RSC3 resurfaced regions are shown in red. CD4i ScFvs are depicted in blue.
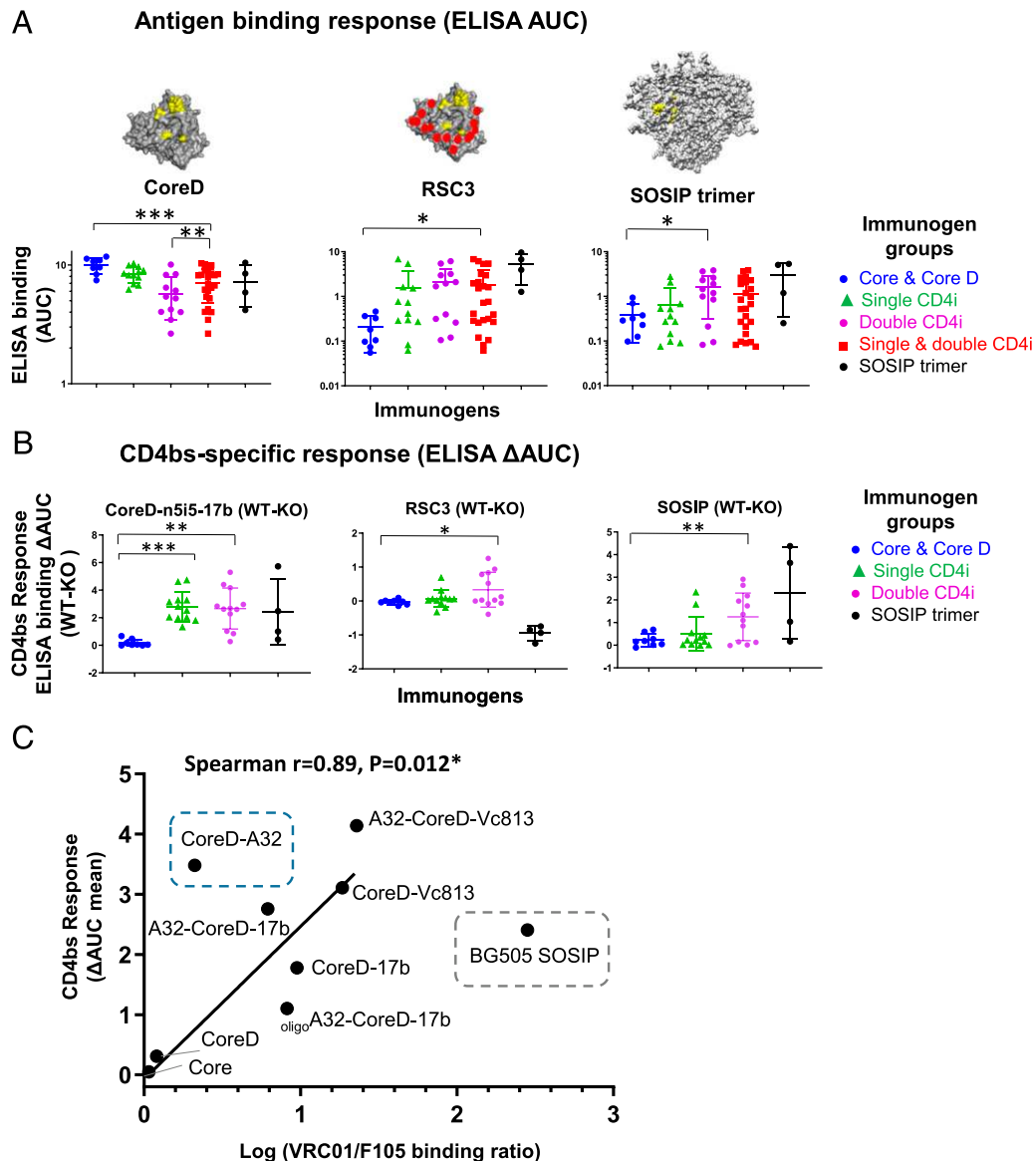
FIGURE 6. Ag binding specificity of the Ab responses in immune mouse sera assessed by ELISA. (**A**) Immune mouse sera (week 11) display various level of binding activity to Ag probes presented as the AUC, shown as mean ± SD. Ag probes include CoreD, RSC3, and BG505 SOSIP trimer. Animal sera were classified into four clusters depending on inoculated immunogens, as shown in Fig. 4 for comparison. Asterisk denotes statistically significant difference. $*p < 0.05$, $**p < 0.01$, $***p < 0.001$, one-way ANOVA. (**B**) CD4bs Ab response of the week 11 immune mouse sera presented as the ELISA binding ΔAUC between the WT Ag probe and the CD4bs KO mutant, CoreD–n5i5–17b WT versus D368R/D474A, RSC3 WT versus ΔRSC3 (Δ371I) (11), and BG505 SOSIP WT versus D368R, respectively, shown as mean ± SD. Statistical analysis result is indicated as in (A). (**C**) The Spearman correlation between CD4bs response [mean ΔAUC in (B)] of week 11 immune sera from mice immunized with individual immunogen and difference of respective immunogen affinity for CD4bs bNAb versus non-bNAb (log K_D [VRC01/F105]), with CoreD–A32 and BG505 SOSIP trimer (denoted in dashed-lined boxes) excluded from the analysis as outliers.

with minimized binding to nonneutralizing, but highly immunogenic, epitopes, including the inner domain and bridging sheets (11). Very weak binding to RSC3 was detected in the sera of animals immunized with Core and CoreD (Fig. 6A, middle; Supplemental Fig. 3B), suggesting that Core immunogens elicited Ab response predominantly to the immunodominant elements that are concealed in the RSC3 probe. Interestingly, the binding titers of the sera from the animals immunized with single and double CD4i-fusion immunogens combined displayed stronger RSC3 binding than those from the Core and CoreD–immunized animals (Fig. 6A, middle; $*p < 0.05$). With the trend even more obvious when probed with the native-like BG505 SOSIP trimer, the sera from mice immunized with double CD4i fusion protein displayed higher binding titers than the Core and CoreD–immunized animals

(Fig. 6A, right, $*p < 0.05$). Therefore, assessment of the sera Ab binding with three different Ag probes suggests that immunization with CoreD–CD4i-fusion proteins elicited quantitatively and qualitatively different response compared with the Core or CoreD alone. This is consistent with the rationale of CD4i fusion protein acting as immunogen; the decreased exposure of nonneutralizing immunodominant elements in CD4i fusion immunogen led to the lower degree of elicitation of Ab response for these immunodominant regions in vivo (Fig. 5C).

CD4i-fusion immunogens focus Ab response to conserved CD4bs bNAb epitopes

Next, we set out to investigate whether the CoreD–CD4i fusion protein immunogens elicited more focused bNAb-like CD4bs–specific

responses than the Core and CoreD immunogens. To gain a better insight into the potential specificity difference of immune sera, we used three Ag probes (resurfaced gp120 Core RSC3, BG505 SOSIP.664 trimer and CD4i fusion protein CoreD–n5i5–17b) and their corresponding CD4bs KO mutants (CD4bs KO) to test the sera binding profiles. As stated previously, these Ag probes enable us to differentiate sera CD4bs-directed Ab response, as they display selective binding for CD4bs bNAbs and their precursors with minimized binding to CD4bs non-bNAbs. We used the difference of the AUC (ΔAUC) between the WT Ag probe and the corresponding CD4bs KO mutant as readouts (Fig. 6B, Supplemental Fig. 3A). Sera from the animals immunized with both single and double CD4i-fusion immunogens displayed statistically significant higher CD4bs bNAbs response than the Core and CoreD immunogen group (Fig. 6B, ***$p < 0.001$, **$p < 0.01$; Supplemental Fig. 3C) when CoreD–n5i5–17b WT and the CD4bs KO (D368R/D474A) mutant were used as Ag probes.

This observation was further corroborated when other selective probes were used to examine the sera CD4bs bNAb responses. With RSC3 and its CD4bs KO mutant (Δ371I) (11) as probes, we detected moderate increase in sera CD4bs bNAb response from the animals immunized with both single and double CD4i-fusion protein immunogens compared with the animals immunized with Core and CoreD (Fig. 6B, Supplemental Fig. 3C), although the difference is statistically significant only for the double CD4i-fusion immunogen group (*$p = 0.011$). Similar result was observed with BG505 SOSIP.664 WT versus D368R mutant (CD4bs KO variant) probe pair (68), whereas sera from animals immunized with double CD4i-fusion group of immunogens demonstrated statistically significant increase of the CD4bs-directed bNAb response compared with that of the Core and CoreD immunogen group. (**$p = 0.004$) (Fig. 6B, Supplemental Fig. 3C). Taken together, the binding patterns of the immunized animal sera with various Env Ag probes demonstrate that CD4i-fusion protein immunogens elicit more focused Ab response to the conserved CD4bs bNAb epitopes than the parental gp120 Core immunogens (Core and CoreD).

To determine if the more CD4bs focused Ab response elicited by the CD4i-fusion protein immunogens attributes to the immunogen antigenicity (e.g., decreased exposure of bridging sheets), we examined if the observed CD4bs-specific Ab response of each immunogen group (Fig. 6B) correlates with the relative affinity of the corresponding immunogens for CD4bs bNAbs versus non-bNAbs (e.g., enhanced binding to bNAb VRC01 and attenuated binding to non-bNAb F105). We found largely a significant correlation (Spearman correlation $r = 0.89$; *$p = 0.012$) between the CD4bs-specific Ab response levels (ΔAUC $_{WT-CD4bs\ KO}$) and the bNAb versus non-bNAb affinity ratio (K_D [VRC01/F105]) of each immunogen (Fig. 6C), with the single CD4i-fusion protein CoreD–A32 and BG505 SOSIP trimer as outliners. Therefore, as expected, the modified antigenicity of CD4i-fusion protein immunogens, particularly the dampened exposure of bridging sheets on gp120 in the presence of CD4i mAb moiety, directs the immune response more focused on the CD4bs bNAb epitopes.

CD4i-fusion proteins elicit B cell response different from the parental immunogens

To delineate the mechanism underlying the more focused CD4bs Ab responses in sera from animals immunized with CoreD–CD4i fusion proteins compared with the parental immunogens, we characterized the B cell response profiles of the CD4bs-directed B cell and memory B cell compartments in the immunized mice. We first determined the frequencies of the CD4bs-specific B cells in the draining (inguinal) lymph nodes of immunized mice, using

CoreD–n5i5–17b WT and the CD4bs KO (D368R/D474A) mutant as probes to identify CD4bs-directed B cells. CD4bs-directed mature B cells were gated as CD19$^+$B220$^+$IgD$^-$CD3$^-$Gr$^-$F4/80$^-$, followed by CoreD–n5i5–17b (WT$^+$ and CD4bs KO$^-$) phenotyping (Fig. 7A). For mice immunized with CoreD-17b, the average CD4bs-directed mature B cell frequency was higher than that of the mice immunized by CoreD–A32 (*$p < 0.05$) and other immunogens (not statistically significant) (Fig. 7A). Oligomeric form of A32–CoreD–17b elicited CD4bs-directed mature B cells at higher frequencies than the monomeric form as well as the parental immunogens, Core and CoreD, although such difference is not statistically significant (Fig. 7A).

Because of the low frequencies of CD4bs-directed B cells in general and the limited number of total lymphocytes per lymph node, we were not able to determine the frequencies of the CD4bs-direcetd B cells in the GC, where they encounter the Ags. However, we were able to assess the frequency of GC B cells by the phenotype of CD19$^+$B220$^+$IgD$^-$CD3$^-$Gr1$^-$F4/80$^-$/GL7$^+$Fas$^+$ (Fig. 7B) and found that the frequency of total GC B cells correlated well with the frequency of CD4bs-directed B cells (Fig. 7C). This observation suggests that, compared with the parental Core/CoreD immunogens, selected CoreD–CD4i fusion protein, such as CoreD–17b, may be able to recruit (or retain) more CD4bs-directed B cells to the GC, a process important for class-switch and affinity maturation.

In addition, we assessed the frequencies of CD4bs-directed memory B cells in immune mice. Memory B cells are subset of B cells that have encountered cognate Ags in the GC and undergone class-switch and affinity maturation, which could respond to subsequent Ag challenge by differentiating to produce Ab (e.g., plasma cells) or return to the GC for another round of GC activation and Ag-driven affinity maturation. We found that mice immunized with CoreD-17b displayed higher frequencies of CD4bs-directed memory B cells, identified as CD19$^+$B220$^+$IgD$^-$IgM$^-$CD3$^-$Gr1$^-$F4/80$^-$CD38$^+$, followed by CoreD–n5i5–17b (WT$^+$ and CD4bs KO$^-$) phenotyping, compared with mice immunized with many other immunogens, such as CoreD and CoreD–A32 (Fig. 7D). This is consistent with the notion that CoreD–17b immunization leads to overall B cells appearing in GC at higher frequency than CoreD immunization (Fig. 7B). Such elevated level of GC activation is important for CD4bs-directed B cell class-switch and affinity maturation, which could result in higher frequency of CD4bs-directed memory B cells than the parental immunogens such as the CoreD.

Isolation of mAbs from mice immunized with double CD4i-fusion protein A32–CoreD–17b

We evaluated the virus neutralization capacity of the sera from the immunized mice with a panel of pseudotype viruses bearing Envs derived from five HIV-1 virus isolates (three tier 1 viruses including HXBc2, MN, and MW965.26 and two tier 2 viruses including 45_01dG5 and BG505) using TZM-bl–based neutralization assays. Briefly, most of the sera displayed neutralization to tier 1 viruses including HXBc2 and MW965.26, whereas neutralization to tier 2 virus 45_01dG5 was weak and sporadic (Supplemental Fig. 4), and no neutralization to tier 1 virus MN and tier 2 virus BG505 was observed (data not shown), which is consistent with the results from previous studies (38, 51). The relatively small serum volume of mice limited our ability to delineate the neutralization specificity against the tier 1 viruses. Nevertheless, our immune sera binding specificity analysis suggest that gp120–CD4i fusion proteins elicit more focused Ab response to the conserved CD4bs bNAb epitopes than parental gp120 Core immunogens (Fig. 6B). Therefore, we set to perform Ag-specific single B cell sorting and
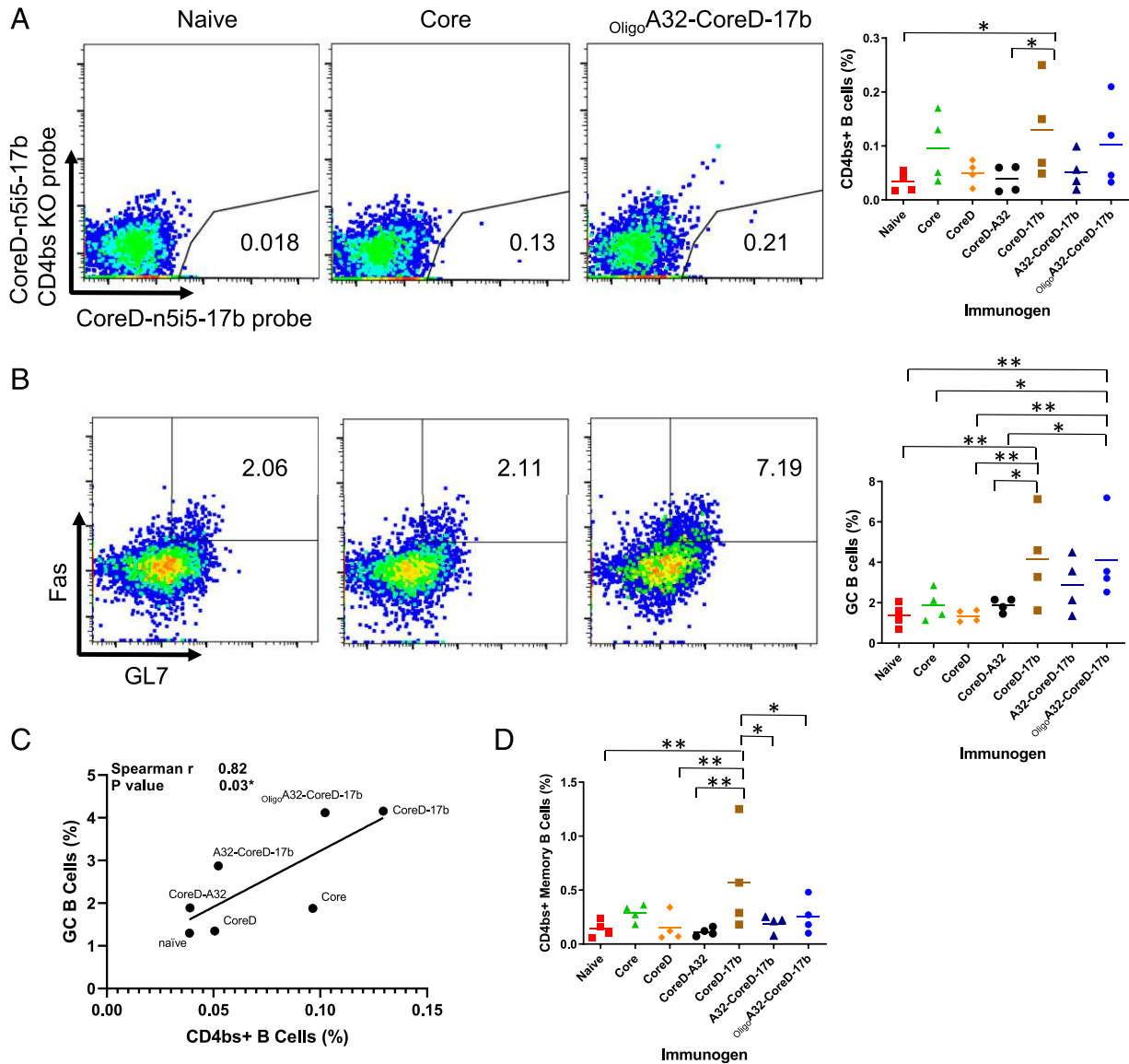
FIGURE 7. GC and CD4bs-directed B cell responses in immune mice. Lymphocytes from draining (inguinal) lymph nodes of immune mice on week 11 were stained with Ag probe and mAbs for surface markers followed by FACS analysis. (**A**) Frequency of CD4bs$^+$ B cells in immune mice, which are initially gated as CD19$^+$B220$^+$CD3$^-$Gr1$^-$F4/80$^-$IgD$^-$, followed by binding phenotype to CD4bs-specific Ag probe pair (CoreD–n5i5–17b WT$^+$ CD4bs KO$^-$). Shown are representative plots. (**B**) Frequency of B cells in GC in immune mice. GC B cells are initially gated as CD19$^+$B220$^+$CD3$^-$Gr1$^-$F4/80$^-$IgD$^-$, followed by GC-specific markers GL7$^+$Fas$^+$. (**C**) Correlation of GC and CD4bs$^+$ B cell frequencies in naive and six immunized animal groups using the nonparametric Spearman test. (**D**) Frequency of CD4bs-directed memory B cells in immune mice. Memory B cells are gated as CD19$^+$B220$^+$CD3$^-$Gr1$^-$F4/80$^-$IgD$^-$CD38$^+$. CD4bs-directed memory B cells are subsequently gates by CD4bs-specific Ag probe pair (CoreD–n5i5–17b WT$^+$ CD4bs KO$^-$) binding phenotype as in (A). $*p < 0.05$, $**p < 0.01$, one-way ANOVA.

cloning to recover individual BCR in soluble IgG form to characterize the immune responses elicited by CD4i-fusion immunogens at clonal level, focused on the CD4bs-directed B cell subset.

Using splenic cells from mice immunized with A32–CoreD–17b protein in monomeric and oligomeric form (Fig. 4A), respectively, we sorted class-switched B cells (CD19$^+$B220$^+$IgD$^-$IgM$^-$) that bound to CoreD–n5i5–17b probe, but not its CD4bs KO variant (Fig. 8A), which represent the CD4bs-directed B cell response and cloned their encoding Ab genes. CD4bs-directed memory B cells were rare, accounting for ~0.8% of the class-switched splenic B cell population (Fig. 8A), similar to the frequencies that we observed in NHP animals previously (52). Two functional mAbs (1A10 and 1A11) were isolated from a mouse immunized with monomeric A32–CoreD–17b, and one (1D3) from a mouse immunized with the immunogen in oligomeric form. V-QUEST

sequence analysis of the mouse mAbs revealed their H (VH) and L chain (VK) V(D)J gene family usages and other VH/VK genetic features (Fig. 8B). These three Abs use distinct V gene segments, suggesting that they are derived from three different clonal lineages. The CDR lengths of their H and L chains range from 12- to 16-aa residues, which are above the average mouse mAb CDRH3 length of 11-aa residues (69). Of note, all three mAbs display low SHM level of both VH/VK segments with 0.3–2.5% for the H chain and 1.4–2.8% for the L chain (nucleotide sequence), respectively, suggesting that they are at the early stages of affinity maturation (Fig. 8B).

As expected, all three mouse mAbs exhibited strong binding to the sorting Ag probe, CoreD–n5i5–17b (Fig. 9A), and no binding to the CoreD–n5i5–17b CD4bs KO mutant (Fig. 9A) in ELISA. Interestingly, the CD4bs bNAb VRC01 shows substantially diminished
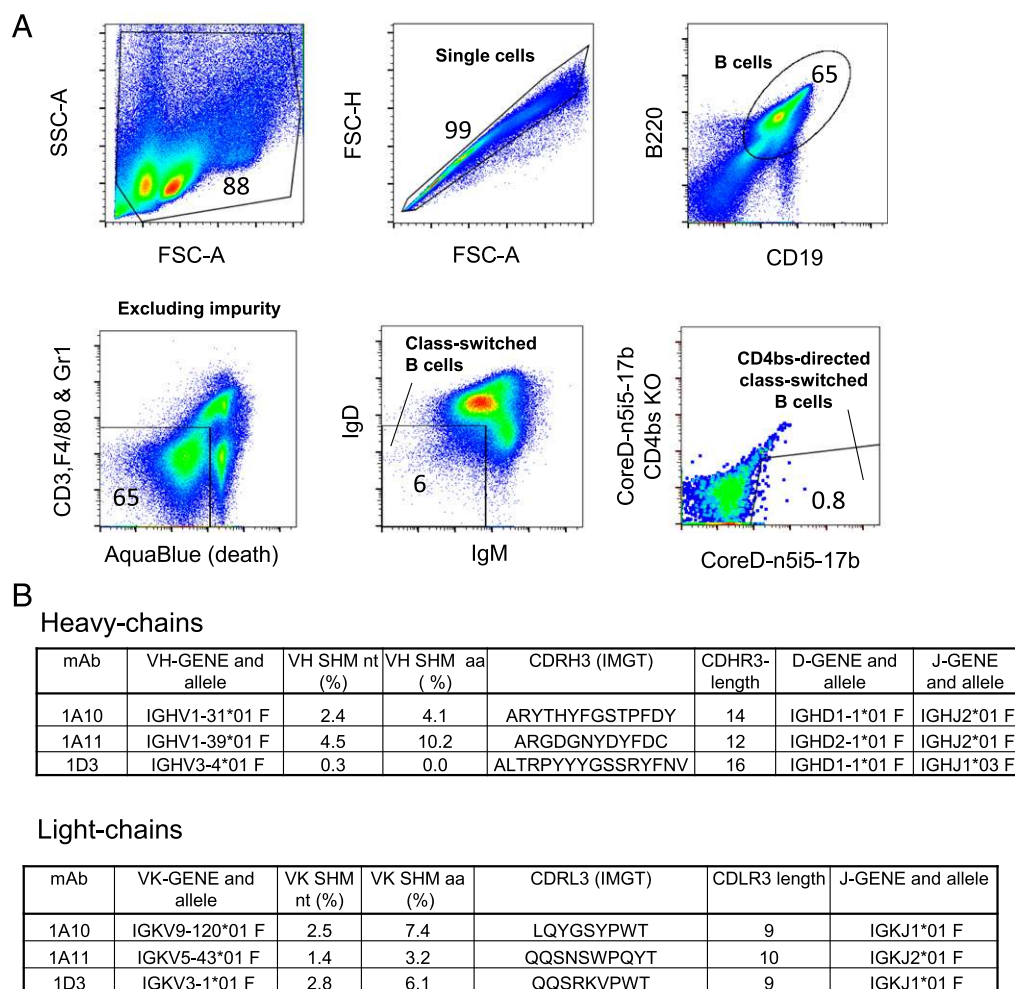
FIGURE 8. Isolation of mAbs from mice immunized with double CD4i-fusion protein A32–CoreD–17b. (**A**) Gating strategy of single-cell sorting for CD4bs-directed class-switched B cells in A32-CoreD-17b-immunized mice. Class-switched B cells were gated as CD19^{+}B220^{+}CD3^{−}Gr1^{−}F4/80^{−} Aqua blue (death)[−]IgM^{−}IgD^{−}, of which CD4bs specificity was indicated by binding phenotype of CoreD–n5i5–17b WT^{+} CD4bs KO^{−} using CoreD–n5i5–17b Ag probes. (**B**) The Ig H and L chain gene family usage and genetic features of three mice mAbs, 1A10, 1A11, and 1D3. SHM presented at both nucleotide (nt) and amino acid sequence (aa) levels. CDRs are delineated according to the ImMunoGeneTics (IMGT) definition.

binding to the CD4bs KO mutant compared with the WT probe (2 logs difference in binding EC_{50} values) (Fig. 9A), similar to these three mouse mAbs, suggesting that they are likely CD4bs directed. In a competition ELISA testing binding to CoreD–n5i5–17b, we observed strong competitions between these mAbs and CD4bs ligands, VRC01 and CD4Ig (Fig. 9B), respectively. Therefore, we confirmed that the epitopes of the mouse mAbs overlapped with those of the well-established CD4bs ligands such as VRC01 and CD4Ig.

Furthermore, we assessed their binding affinities for additional Env ligands. All of the three CD4bs-directed mouse mAbs displayed strong binding to Ags with glycan 276 and 463 deletion (glycan 276/463[off]) including double CD4i-fusion protein immunogens (Fig. 9C), and modest to strong binding to CoreD (Fig. 9C). However, their binding to Core with intact 276 and 463 glycans (glycan 276/463[on]) in the vicinity of CD4bs was attenuated for 1D3 and abolished for 1A10 and 1A11 (Fig. 9C), respectively. Furthermore, unlike bNAb VRC01, these three mouse CD4bs mAbs showed no binding to other glycan 276/463[on] Ags, such as the resurfaced gp120 Core, RSC3, and the native-like trimer BG505 SOSIOP.664 (Fig. 9C). Poor binding of the mouse CD4bs mAbs to gp120 ligands with intact loop D (276) and V5 (463) glycans suggests that they fail to overcome the steric barrier imposed by the glycans surrounding the CD4bs epitope in

the full-length gp120 Core as well as the Env trimer. However, the binding affinities of these three mouse mAbs to the cognate immunogen A32–CoreD–17b, and the sorting probe CoreD–n5i5–17b are substantial (ranging from 20 to 50 nM) (Fig. 9D), suggesting that sufficient affinity maturation of the mouse mAbs has been achieved with the concurrent immunization regimen (three immunizations with one single immunogen lack of glycans 276 and 463) despite of the moderate SHM level in the corresponding Ig VH/VL gene segments. Therefore, subsequent booster immunizations with Env trimer immunogens bearing such glycans may be performed to drive additional Ig gene affinity maturation that are required for these Abs to overcome glycan steric barriers on the native Env trimers (62).

Mouse CD4bs mAbs show Env binding footprints comparable with VRC01-class Ab

Next, we sought to determine the Env CD4bs epitope residues critical for binding the mouse CD4bs mAbs with a panel of CoreD–n5i5–17b mutant variants bearing point mutations on selected Env residues within this epitope (Fig. 10). Selection criteria of the key residues in CD4bs bNAb epitope were derived from previous structural and functional studies (11, 24, 34), showing mutations at VRC01-like bNAb contact residues in loop D, the CD4 binding loop (CD4 BLP), V5, and C5 (β24–α5 connection) region of Env
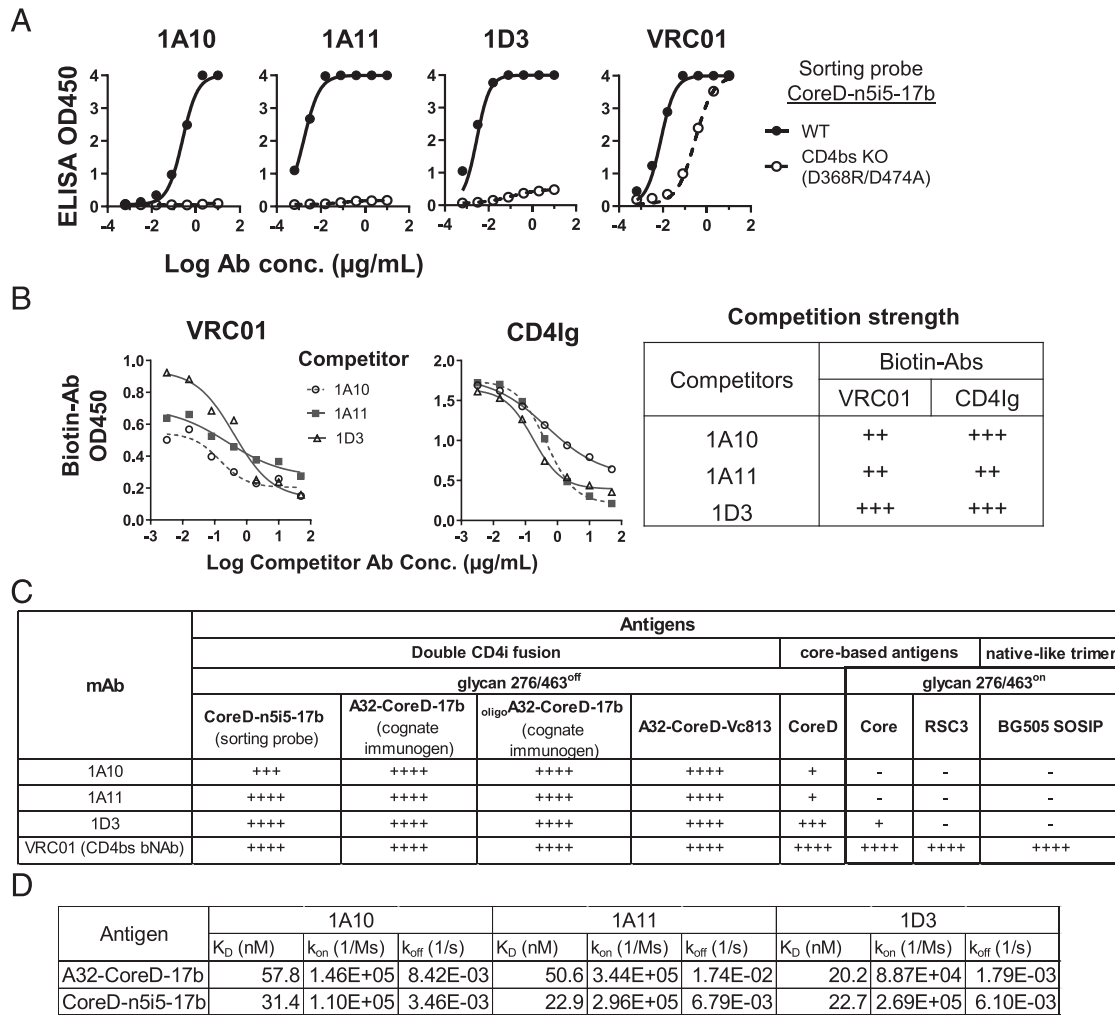
A

Panel A: ELISA OD450 vs Log Ab conc. (µg/mL) for 1A10, 1A11, 1D3, VRC01.

Sorting probe CoreD-n5i5-17b
- ● WT
- ○ CD4bs KO (D368R/D474A)

B

Panel B: Biotin-Ab OD450 vs Log Competitor Ab Conc. (µg/mL) for VRC01 and CD4Ig.

Competitor:
- ○ 1A10
- ■ 1A11
- △ 1D3

Competition strength

Competitors	Biotin-Abs	
	VRC01	CD4Ig
1A10	++	+++
1A11	++	++
1D3	+++	+++

C

mAb	Antigens							
	Double CD4i fusion				core-based antigens			native-like trimer
	glycan 276/463off				glycan 276/463on			
	CoreD-n5i5-17b (sorting probe)	A32-CoreD-17b (cognate immunogen)	oligoA32-CoreD-17b (cognate immunogen)	A32-CoreD-Vc813	CoreD	Core	RSC3	BG505 SOSIP
1A10	+++	++++	++++	++++	+	-	-	-
1A11	++++	++++	++++	++++	+	-	-	-
1D3	++++	++++	++++	++++	+++	+	-	-
VRC01 (CD4bs bNAb)	++++	++++	++++	++++	++++	++++	++++	++++

D

Antigen	1A10			1A11			1D3		
	K_D (nM)	k_{on} (1/Ms)	k_{off} (1/s)	K_D (nM)	k_{on} (1/Ms)	k_{off} (1/s)	K_D (nM)	k_{on} (1/Ms)	k_{off} (1/s)
A32-CoreD-17b	57.8	1.46E+05	8.42E-03	50.6	3.44E+05	1.74E-02	20.2	8.87E+04	1.79E-03
CoreD-n5i5-17b	31.4	1.10E+05	3.46E-03	22.9	2.96E+05	6.79E-03	22.7	2.69E+05	6.10E-03

FIGURE 9. Ag-binding specificities of mAbs from mice immunized with double CD4i-fusion protein A32–CoreD–17b. (**A**) Mouse mAbs (1A10, 1A11, and 1D3) display similar binding specificity with CD4bs bNAb VRC01 to sorting probes, CoreD–n5i5–17b WT and CD4bs KO mutant, D368R/D474A, by ELISA. (**B**) Competition of biotin-labeled prototypical CD4bs ligands, VRC01 (left) and CD4Ig (right), respectively, with mouse mAbs as competitor for binding to CoreD–n5i5–17b. +++, 75–100% competition; ++, 50–75% competition. (**C**) ELISA binding profiles of mouse mAbs to various Ags, with intact 276 and 463 glycans (glycan 276/463on) or removed (glycan 276/463off). Binding was categorized based on OD_{450} values at the highest concentration of mAb and the EC_{50} (µg/ml) values. ++++, $OD_{450} > 3.0$, $EC_{50} < 0.1$; +++, $OD_{450} > 3.0$, $EC_{50} > 0.1$; ++, $1.0 < OD_{450} < 3.0$; +, $0.2 < OD_{450} < 1.0$; −, $OD_{450} < 0.2$. (**D**) Kinetic parameters of mouse mAbs binding to gp120–CD4i fusion proteins assessed by BLI. k_{on}, k_{off}, and K_D are defined as in Fig. 2C.

substantially decreased VRC01 binding or neutralization (Fig. 10A). To the end, we constructed and expressed seven variants of CoreD–n5i5–17b with mutations situated within the VRC01-like CD4bs bNAb epitope (Fig. 10B) for fine mapping the epitopes of these mouse CD4bs mAbs.

To quantify the effect of these mutations on the binding of mouse mAbs and several human CD4bs bNAbs, we calculated the areas under the BLI binding curves (AUC, Fig. 10B). CoreD–n5i5–17b mutant-binding affinity relative to WT (in percentage) for each CD4bs mAb was calculated as (AUC_CoreD–n5i5–17b mutant/ AUC_CoreD–n5i5–17b WT) ×100. We used well-characterized CD4bs bNAbs (VRC01, VRC03, VRC06, and PGV04), CD4Ig, the surrogate of receptor CD4, and the immature VRC01 bNAb precursor, VRC01GL, for epitope mapping comparison. The fine-mapping data suggested that the Env regions targeted by mouse mAbs extensively overlap with the contact residues of human VRC01-class bNAbs on Env (Fig. 10B). Of note, mutations D276N and D276N/D463N, designed to restore the loop D and loop D/V5 glycans, respectively, substantially impeded the binding of the mouse mAbs and most CD4bs bNAbs to CoreD–n5i5–17b

(Fig. 10B). Similar observation was obtained for the binding of bNAb precursor, VRC01GL to these glycan-restoring mutants (Fig. 10B). Therefore, the Ag binding of the mouse mAbs is sensitive to mutations of most of the critical Env residues within the CD4bs epitope (Fig. 10B), largely resembling the VRC01-class CD4bs bNAbs and representative precursor VRC01GL.

In a color-coded manner, we illustrated the relative binding affinity (Fig. 10B) of the mouse mAbs to the WT Ag probe CoreD–n5i5–17b and each mutant on the surface of the CoreD–n5i5–17b model (Fig. 10C) to visualize the corresponding Ab-contacting residues, in comparison with the VRC01-class CD4bs bNAbs. The most striking similarity can be observed between the footprints of mouse mAb 1A10 and the immature VRC01 precursor, VRC01GL (Fig. 10C). All of the mutations completely abolished CoreD–n5i5–17b binding to both mAbs. The epitopes of other mouse mAbs (1A11 and 1D3) turned out to be more similar to the mature CD4bs bNAbs (Fig. 10C), than that of VRC01GL. Overall, the epitope fine-mapping data indicate that the vaccine-induced mouse mAbs target envelope regions similar to those of the well-characterized CD4bs bNAbs.
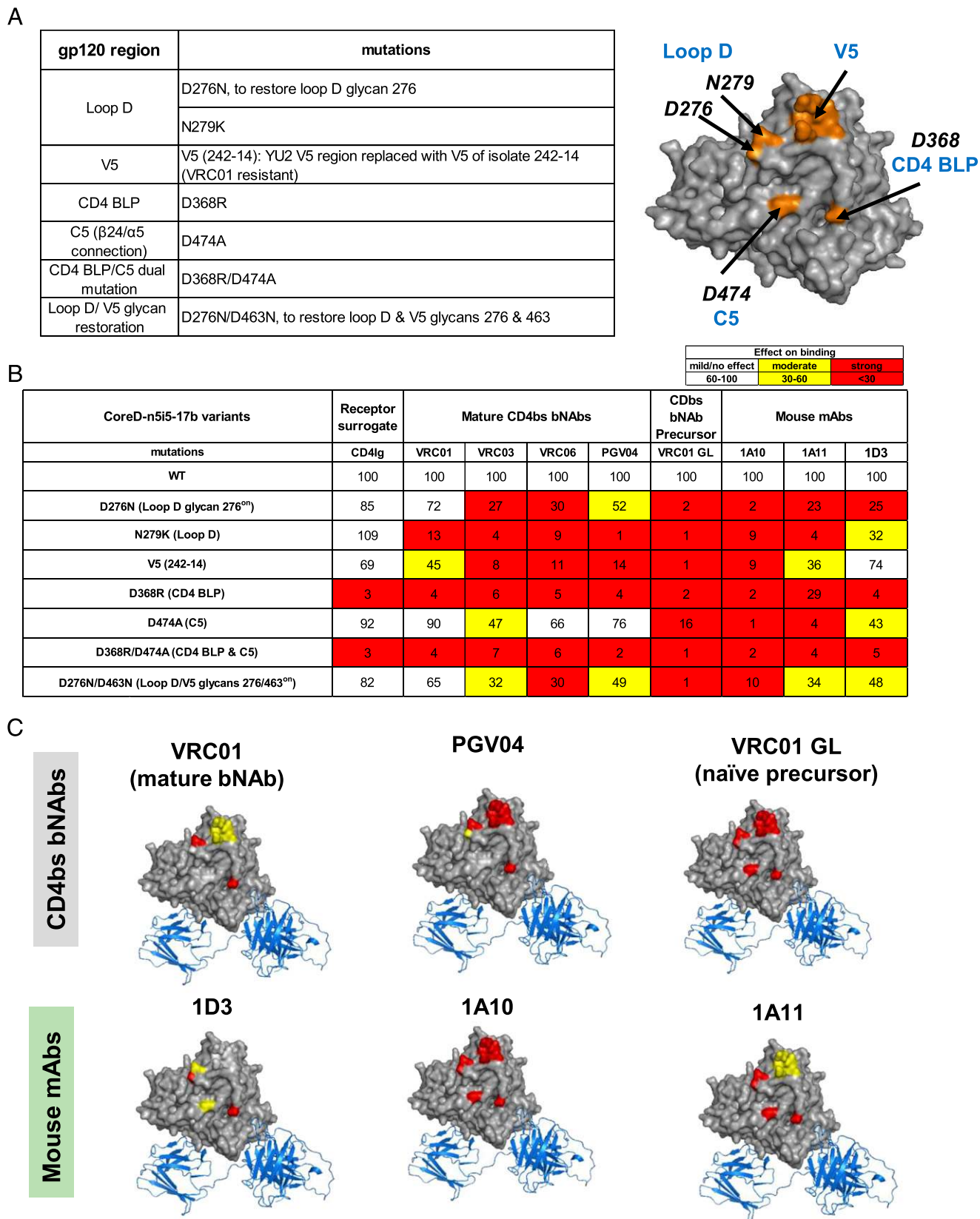
A

gp120 region	mutations
Loop D	D276N, to restore loop D glycan 276
	N279K
V5	V5 (242-14): YU2 V5 region replaced with V5 of isolate 242-14 (VRC01 resistant)
CD4 BLP	D368R
C5 (β24/α5 connection)	D474A
CD4 BLP/C5 dual mutation	D368R/D474A
Loop D/ V5 glycan restoration	D276N/D463N, to restore loop D & V5 glycans 276 & 463

B

			Effect on binding	
	mild/no effect	moderate		strong
	60-100	30-60		<30

CoreD-n5i5-17b variants	Receptor surrogate	Mature CD4bs bNAbs				CDbs bNAb Precursor	Mouse mAbs		
mutations	CD4Ig	VRC01	VRC03	VRC06	PGV04	VRC01 GL	1A10	1A11	1D3
WT	100	100	100	100	100	100	100	100	100
D276N (Loop D glycan 276^{on})	85	72	27	30	52	2	2	23	25
N279K (Loop D)	109	13	4	9	1	1	9	4	32
V5 (242-14)	69	45	8	11	14	1	9	36	74
D368R (CD4 BLP)	3	4	6	5	4	2	2	29	4
D474A (C5)	92	90	47	66	76	16	1	4	43
D368R/D474A (CD4 BLP & C5)	3	4	7	6	2	1	2	4	5
D276N/D463N (Loop D/V5 glycans 276/463^{on})	82	65	32	30	49	1	10	34	48

C

CD4bs bNAbs

VRC01 (mature bNAb)　　**PGV04**　　**VRC01 GL (naïve precursor)**

Mouse mAbs

1D3　　**1A10**　　**1A11**

FIGURE 10. The footprints of mouse CD4bs mAbs on Env surface determined by differential binding to selected CD4bs mutants of Ag CoreD–n5i5–17b. (**A**) A mini panel of CoreD–n5i5–17b mutants for fine mapping the critical contact residues in the Env CD4bs region for mouse mAb recognition. Left, a list of the mutations in the context of CoreD–n5i5–17b sequence; right, the residues with mutations used for CD4bs mapping are highlighted in orange on the YU2 gp120 Core molecular surface (PDB: 3tgq). Four Env major regions involved in CD4bs bNAb binding are marked in blue: loop D, V5, CD4 BLP (CD4 binding loop), and C5. (**B**) Binding affinity of CoreD–n5i5–17b mutant Ags with various CD4bs bNAbs and mouse mAbs relative to the WT CoreD–n5i5–17b, is presented in percentage (%) and color-coded. The relative binding affinity was assessed by BLI. (**C**) Summary of mouse CD4bs mAb footprints on the surface of CoreD–n5i5–17b, in comparison with mature CD4bs bNAbs, VRC01 and PGV04, and naive precursor, VRC01GL, as determined in (B). The effect of mutations on Ab binding is color coded as in (B).

The angle of approach to Env deployed by 1D3 revealed by SAXS analysis

Prior structural studies revealed that bNAbs oftentimes use unique angles to approach their cognate epitopes to minimize steric hindrance imposed by Env structural elements (27, 36). VRC01-class CD4bs bNAbs approach their epitopes at a more favorable angle than other CD4bs non-bNAbs (34, 36, 55). The relative orientation of the binding partners is restricted by the steric constraints imposed by structural elements including the variable loops and the neighboring subunits (protomers) of the Env trimer spike. Our finding that mAbs isolated from mice immunized with A32–CoreD–17b exhibited footprints comparable with VRC01-class bNAbs indicates that they may share some degree of similarity in the angle of approach to the CD4bs epitope.

To examine the binding mode of mouse mAbs to their cognate CD4bs epitopes, we collected solution SAXS data for CoreD–n5i5–17b complexed with the Fabs of VRC01 and 1D3, respectively (Fig. 11). We authenticated our experimental x-ray scattering data by inspecting a number of critical relevant parameters of the complex samples, including their high degree of monospersity, m.w., and particle dimensions (Table I), which are all in good agreement with the expected values. We then used two complementary approaches for the structural interpretation of SAXS data.

First, we evaluated the agreement of the all-atom models of the complexes (independently generated) against the experimental scattering data. The all-atom model is the approach with top-ranked accuracy for structure-based SAXS data prediction. The all-atom models of the VRC01 or 1D3 Fab in complex with CoreD–n5i5–17b is in good agreement with the experimental SAXS data (fit parameter, $\chi = 1.36$ and 1.21, respectively) (Fig. 11A).

In the second approach, the all-atom models of the VRC01 Fab or 1D3 Fab:CoreD–n5i5–17b complex were validated by reconstructing low-resolution ab initio envelope shapes from the experimental SAXS data (see *Materials and Methods* section for details), which is completely unbiased in terms of the structural model and can thus detect the presence of multiple structural solutions with similar fits to the scattering data. There are 10 ab initio models for each of the VRC01 or 1D3 Fab:CoreD–n5i5–17b complex generated with different initial random number seeds, which are in good agreement with the experimental scattering profile. We then used the averaged and consistency-filtered ab initio (DAMMIN bead) models to calculate the overall molecular surfaces of these complexes displayed in Fig. 11B.

Both approaches produced consistent results, suggesting general reliability of the relative orientations of the CD4bs mAb Fabs within the two complexes. Importantly, both datasets clearly show differences between the VRC01 and 1D3 positions within the reconstructed low-resolution shapes of the complex (Fig. 11B, right panel), supporting significant divergence in the angle of approach of the two mAbs with respect to the CoreD–n5i5–17b; the angle of approach used by VRC01 is more lateral than that by 1D3 (Fig. 11B, right panel). We then compared the binding modes and angles of approach to cognate CD4bs epitopes used by VRC01, 1D3, and non-bNAb F105 (PDB: 3hi1) in the context of the Env trimer (PDB: 5fyj) (Fig. 11C) modeled by Chimera (46). Overall, VRC01 and 1D3 are positioned more distal from the Env trimer apex than CD4bs non-bNAb F105 (Fig. 11C). Moreover, the longitudinal angle of approach for bNAb VRC01 or mouse mAb 1D3 to CD4bs is different from that for F105 (Fig. 11C, left). Obviously, the L chain of F105 clashes with the bridging sheet shielded by the variable-loop cluster at the trimer apex, as described previously (37, 38) (Fig. 11C, right). However, this steric

clash can be avoided by VRC01 and 1D3 mAbs because of their angles of approach and footprint shifts (Fig. 11C, left) different from F105. Thus, 1D3, elicited by the Core-CD4i fusion protein samples an angle of approach to CD4bs different from the non-bNAb F105, consistent with the rationale of using core-CD4i fusion protein to counter select CD4bs non-bNAb B cell clones, such as F105, that use vertical approaching angle for Env and substantially contact Env bridging sheet and inner domain (38).

Discussion

In this study, we designed gp120–CD4i fusion protein as immunogens to improve the elicitation of CD4bs bNAb response by selective elimination of glycans flanking the CD4bs to increase the CD4bs exposure while blocking the immunodominant non-bNAb epitopes by including CD4i mAb functional moieties as immunogen component. We tested the immunogenicity of these gp120–CD4i fusion proteins in mice, which revealed focused elicitation of CD4bs Ab response in sera from animals immunized with gp120–CD4i fusion proteins compared with gp120 Core, as evident by preferential binding to various Env probes specifically presenting CD4bs epitopes (Fig. 6). Consistently, sera from animals immunized with CD4i fusion proteins displayed higher binding titers to native-like trimer BG505 SOSIP.664 than those immunized with the gp120 Core, indicating that gp120–CD4i fusion proteins elicit Ab response with higher potential of penetrating the Env functional trimer than gp120 Core. Furthermore, we found that mice immunized with selected gp120–CD4i fusion proteins have higher frequencies of GC-activated B cells and CD4bs-directed memory B cells than those inoculated with parental immunogens. The elevated level of GC B cell activation conferred by selected gp120–CD4i fusion protein immunogens is particularly promising for recruiting and retaining CD4bs bNAb precursors that oftentimes exist at low frequencies to the GC for the affinity maturation process driven by Ag selection. The improved frequency of CD4bs-directed memory B cells in selected gp120–CD4i fusion protein–immune mice indicates that the resulted B cell response may have elongated longevity as well as stronger response to Ag recall. Therefore, we expect that gp120–CD4i fusion proteins could be used as immunogens to target the CD4bs bNAb epitope more efficiently and precisely than the parental immunogens.

In contrast, despite the observed more focused CD4bs-direcetd Ab response in mice immunized with gp120–CD4i fusion proteins, this type of CD4bs-direcetd Ab responses did not show the ability to mediate tier 2 virus neutralization of breadth, presumably because of the limited affinity maturation established by the current immunization regimen. It is likely that such response, as represented by the three CD4bs-directed mAbs with VRC01-like footprints and approaching angles distinct from predominant CD4bs non-bNAbs, has been primed by gp120–CD4i fusion proteins but yet to be shepherded toward bNAb response through further affinity maturation process. Future work using transgenic mice expressing precursors of human CD4bs bNAbs (70, 71) to study the elicitation of VRC01-class bNAb response by gp120–CD4i fusion protein immunogens will be informative, as bNAb precursors are generally rare or of paucity in WT mice (28, 72).

Previous immunogenicity studies of HIV-1 vaccine candidates strongly suggest that elicitation of cross-reactive NAbs requires sequential immunization regimen (26, 66, 73–77) rather than immunizations with a single immunogen. In this immunization scenario, targeting of a desirable epitope (e.g., CD4bs) is achieved via the following: 1) priming/activating cognate naive B cell germline precursors with germline-targeting immunogen, followed by 2) a series of shepherding immunizations to drive affinity maturation of the intermediate B cell precursors toward cross-reactivity with
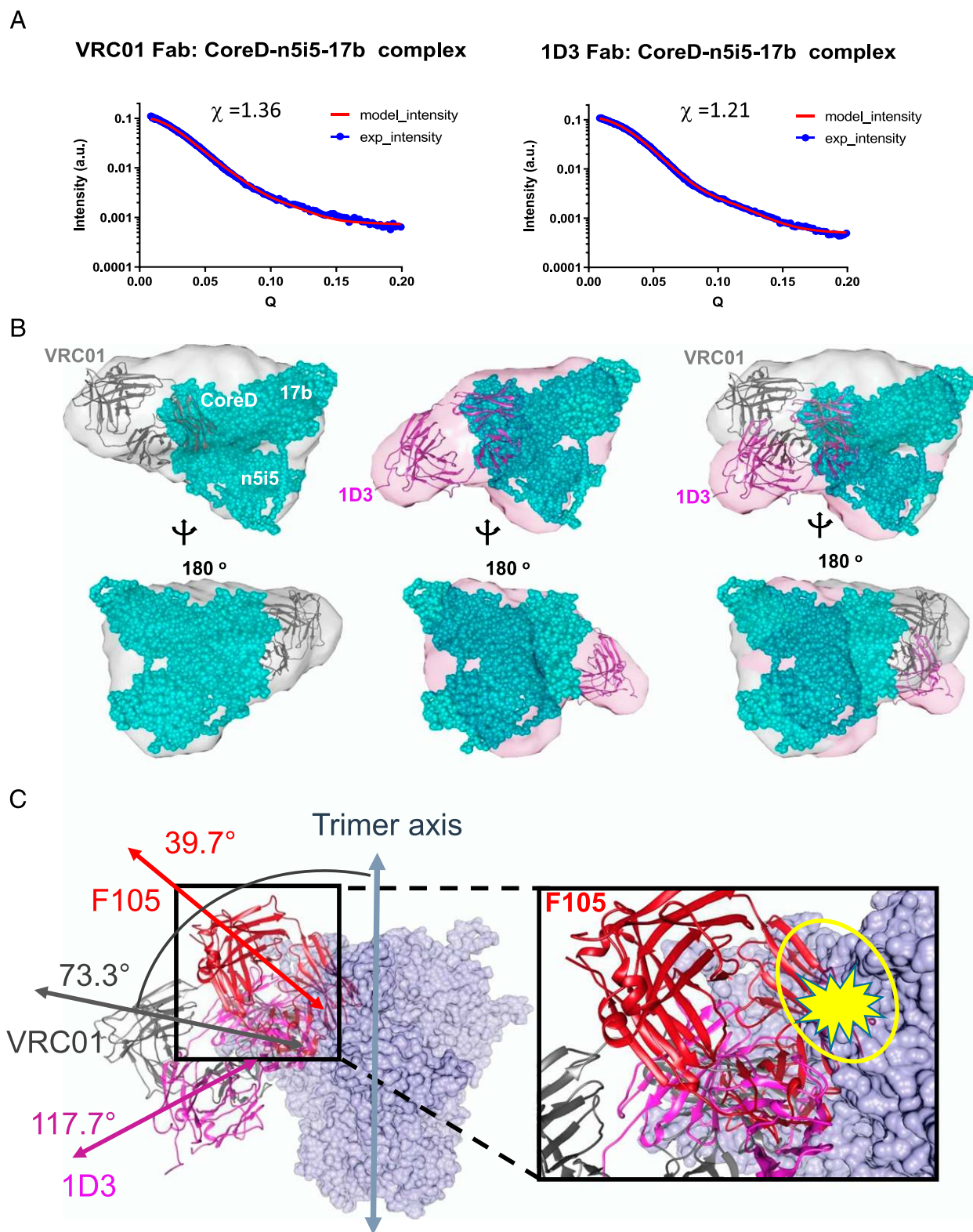
FIGURE 11. Env-binding mode similarity and divergence between mouse CD4bs mAb 1D3 and bNAb VRC01. (**A**) Fits of SAXS experimental data (blue) to all-atom models (red) of VRC01 Fab (left) or 1D3 Fab (right) complexed with CoreD–n5i5–17b. VRC01 Fab position was derived from experimental x-ray structure of VRC01 Fab: gp120 Core complex (PDB: 3ngb). 1D3 Fab binding mode to CoreD–n5i5–17b was predicted with Rosetta docking and fit into the experimental SAXS scattering curve. (**B**) Molecular shapes (shown as transparent surfaces) of VRC01 or 1D3 Fab: CoreD–n5i5–17b complexes determined by SAXS and aligned with representative all-atom structures. VRC01 complex is shown in light gray; 1D3 complex is in light magenta. Envelopes were drawn over the filtered averaged DAMMIN structures. All-atom structural models of the complexes were overlaid and fit into the SAXS density with Chimera for comparison. The CoreD–n5i5–17b model is shown in cyan spheres, and VRC01 (gray) and 1D3 (magenta) Fabs are shown as cartoons. (**C**) Binding mode of mouse and human CD4bs mAbs in the context of Env trimer, shown as a light blue semitransparent surface. Angle of approach of CD4bs non-NAb F105 (defined as the angle between the Ab and trimer axis) is different from that of bNAb VRC01 or mouse 1D3 Abs. Models of the complexes with VRC01 (gray), 1D3 (light magenta), and F105 (red) were superposed using common gp120 Core unit with Chimera (46). In the right-side insert, the steric clash of the F105 L chain with the trimer apex loop cluster is denoted in a yellow circle.

Table I. SAXS-extracted size parameters for the mAb Fabs and Fab–Ag complexes

Protein Sample	$R_{gyr}^{Guinier}$ (Å)	R_{gyr}^{GNOM} (Å)	D_{max}^{GNOM} (Å)	MW^{SAXS} (kDa)	$MW^{Expected}$ (kDa)
VRC01 Fab	28.7 ± 0.2	28.8 ± 0.2	101 ± 5	67 ± 6	51.1
1D3 Fab	26.3 ± 0.2	26.3 ± 0.1	91 ± 6	59 ± 5	49. 2
VRC01:CoreD–n5i5–17b complex	51.4 ± 0.9	51.3 ± 0.3	176 ± 7	166 ± 17	152.8
1D3:CoreD–n5i5–17b complex	50.3 ± 1.1	50.1 ± 0.3	165 ± 6	154 ± 16	150.7

D_{max}^{GNOM}, extracted maximum dimension of the scattering complex particles; $MW^{Expected}$, molecular mass of test proteins derived from corresponding amino acid sequence; MW^{SAXS}, molecular mass of the scattering complex particles calculated using the $I(Q = 0)$ relative to the measured scattering intensity of bulk water sample from SAXS data; R_{gyr}^{GNOM}, radius of gyration obtained by the Fourier transforms of the complete scattering curves; $R_{gyr}^{Guinier}$, radius of gyration extracted from the lowest-angle data.

diverse viral Env spikes, and 3) a final boost to expand the desirable cross-reactive clones to elicit the bNAb Ab response. Selected gp120–CD4i fusion proteins designed in our study could be used as immunogens in this scenario. As shown earlier, our gp120–CD4i fusion proteins display affinity for VRC01 germline precursor (VRC01GL) ranging from 60 to 200 nM, which is sufficient to prime VRC01-class germline precursors in vivo (71). Further modifications such as multivalent presentation of these gp120–CD4i fusion proteins could enhance the priming efficiency (78, 79).

Two types of priming immunogens have been generated by previous studies, which include the outer domain-based immunogens (exemplified by eOD-GT6 and eOD-GT8) engineered from tier 1 HXBc2 gp120 outer domain with deletion of the whole inner domain, and Env variants derived from tier 2 viruses 426c (28, 29, 78, 79) and BG505 (80, 81). Consisting of gp120 Core derived from primary isolate YU2 and possessing intact Env inner domain, our gp120–CD4i fusion proteins are different from these germline-targeting immunogens. The inclusion of inner domain in our gp120–CD4i fusion proteins may render the CD4bs epitope situating in a structural context more mimicking the intact Env than eOD GT immunogens, and thus able to impose proper selective pressure for bNAb precursors. The CD4i moieties covalently connected with the gp120 Core with flexible linker, which mask the immunodominant determinants on the bridging sheet and inner domain could facilitate immunofocusing conferred by the gp120–CD4i fusion proteins, a unique feature distinguishing it from the 426c or BG505 Env-based priming immunogens.

In addition to priming naive bNAb B cell precursors, our gp120–CD4i fusion proteins could serve as intermediate shepherding immunogens as well as the "final polishing" immunogen to expand desirable bNAb clonal lineages. Recent structural and functional studies reveal that variable loops (82) and N-linked glycans (28, 29, 62) on Env impose substantial steric hindrance for bNAb and precursors. In this study, we selectively removed N-linked glycan 276 in loop D as well as glycan 463 in the V5 region in our gp120 Core to facilitate better activation of VRC01-class Abs as suggested by previous studies (28, 29). Of note, these glycans have high prevalence in the Env functional spike of primary virus isolates (27). Thus, these glycans need present in the intermediate shepherding and final polishing immunogens to select bNAb clones that can overcome the glycan steric hindrance and confer potent virus neutralization. Our gp120–CD4i fusion proteins, modified to bear the 276/463 glycans, could be applied in conjunction with the well-ordered Env trimers as shepherding and final polishing immunogens to select the bNAb clones capable of overcoming the key glycans profoundly limiting the breadth of NAb response (62). Additional studies rationalizing the combinations and permutations of boosting immunizations are required to establish a series of immunizations with succession of related immunogens, as suggested by previous work on the successful induction of PGT121-like bNAb response (76), which could lead to augmented elicitation of CD4bs-directed bNAb responses via vaccination.

Disclosures

The authors have no financial conflicts of interest.

References

1. Wyatt, R., and J. Sodroski. 1998. The HIV-1 envelope glycoproteins: fusogens, antigens, and immunogens. *Science* 280: 1884–1888.
2. Wu, L., N. P. Gerard, R. Wyatt, H. Choe, C. Parolin, N. Ruffing, A. Borsetti, A. A. Cardoso, E. Desjardin, W. Newman, et al. 1996. CD4-induced interaction of primary HIV-1 gp120 glycoproteins with the chemokine receptor CCR-5. *Nature* 384: 179–183.
3. Kwong, P. D., R. Wyatt, J. Robinson, R. W. Sweet, J. Sodroski, and W. A. Hendrickson. 1998. Structure of an HIV gp120 envelope glycoprotein in complex with the CD4 receptor and a neutralizing human antibody. *Nature* 393: 648–659.
4. Pancera, M., T. Zhou, A. Druz, I. S. Georgiev, C. Soto, J. Gorman, J. Huang, P. Acharya, G. Y. Chuang, G. Ofek, et al. 2014. Structure and immune recognition of trimeric pre-fusion HIV-1 Env. *Nature* 514: 455–461.
5. Li, Y., S. A. Migueles, B. Welcher, K. Svehla, A. Phogat, M. K. Louder, X. Wu, G. M. Shaw, M. Connors, R. T. Wyatt, and J. R. Mascola. 2007. Broad HIV-1 neutralization mediated by CD4-binding site antibodies. *Nat. Med.* 13: 1032–1034.
6. Walker, L. M., M. D. Simek, F. Priddy, J. S. Gach, D. Wagner, M. B. Zwick, S. K. Phogat, P. Poignard, and D. R. Burton. 2010. A limited number of antibody specificities mediate broad and potent serum neutralization in selected HIV-1 infected individuals. *PLoS Pathog.* 6: e1001028.
7. Lynch, R. M., L. Tran, M. K. Louder, S. D. Schmidt, M. Cohen, R. Dersimonian, Z. Euler, E. S. Gray, S. Abdool Karim, J. Kirchherr, et al; CHAVI 001 Clinical Team Members. 2012. The development of CD4 binding site antibodies during HIV-1 infection. *J. Virol.* 86: 7588–7595.
8. Landais, E., X. Huang, C. Havenar-Daughton, B. Murrell, M. A. Price, L. Wickramasinghe, A. Ramos, C. B. Bian, M. Simek, S. Allen, et al. 2016. Broadly neutralizing antibody responses in a large longitudinal sub-saharan HIV primary infection cohort. *PLoS Pathog.* 12: e1005369.
9. Rusert, P., R. D. Kouyos, C. Kadelka, H. Ebner, M. Schanz, M. Huber, D. L. Braun, N. Hozé, A. Scherrer, C. Magnus, et al; Swiss HIV Cohort Study. 2016. Determinants of HIV-1 broadly neutralizing antibody induction. *Nat. Med.* 22: 1260–1267.
10. Scheid, J. F., H. Mouquet, B. Ueberheide, R. Diskin, F. Klein, T. Y. Oliveira, J. Pietzsch, D. Fenyo, A. Abadir, K. Velinzon, et al. 2011. Sequence and structural convergence of broad and potent HIV antibodies that mimic CD4 binding. *Science* 333: 1633–1637.
11. Wu, X., Z. Y. Yang, Y. Li, C. M. Hogerkorp, W. R. Schief, M. S. Seaman, T. Zhou, S. D. Schmidt, L. Wu, L. Xu, et al. 2010. Rational design of envelope identifies broadly neutralizing human monoclonal antibodies to HIV-1. *Science* 329: 856–861.
12. Huang, J., B. H. Kang, E. Ishida, T. Zhou, T. Griesman, Z. Sheng, F. Wu, N. A. Doria-Rose, B. Zhang, K. McKee, et al. 2016. Identification of a CD4-binding-site antibody to HIV that evolved near-*Pan* neutralization breadth. *Immunity* 45: 1108–1121.
13. Sajadi, M. M., A. Dashti, Z. Rikhtegaran Tehrani, W. D. Tolbert, M. S. Seaman, X. Ouyang, N. Gohain, M. Pazgier, D. Kim, G. Cavet, et al. 2018. Identification

of Near-Pan-neutralizing Antibodies against HIV-1 by Deconvolution of Plasma Humoral Responses. *Cell* 173: 1783–1795.e14.

14. Walker, L. M., S. K. Phogat, P. Y. Chan-Hui, D. Wagner, P. Phung, J. L. Goss, T. Wrin, M. D. Simek, S. Fling, J. L. Mitcham, et al; Protocol G Principal Investigators. 2009. Broad and potent neutralizing antibodies from an African donor reveal a new HIV-1 vaccine target. *Science* 326: 285–289.

15. Zhou, T., R. M. Lynch, L. Chen, P. Acharya, X. Wu, N. A. Doria-Rose, M. G. Joyce, D. Lingwood, C. Soto, R. T. Bailer, et al; NISC Comparative Sequencing Program. 2015. Structural repertoire of HIV-1-Neutralizing antibodies targeting the CD4 supersite in 14 donors. *Cell* 161: 1280–1292.

16. Umotoy, J., B. S. Bagaya, C. Joyce, T. Schiffner, S. Menis, K. L. Saye-Francisco, T. Biddle, S. Mohan, T. Vollbrecht, O. Kalyuzhniy, et al. 2019. Rapid and focused maturation of a VRC01-class HIV broadly neutralizing antibody lineage involves both binding and accommodation of the N276-glycan. *Immunity* 51: 141–154.e6.

17. Sanders, R. W., R. Derking, A. Cupo, J. P. Julien, A. Yasmeen, N. de Val, H. J. Kim, C. Blattner, A. T. de la Peña, J. Korzun, et al. 2013. A next-generation cleaved, soluble HIV-1 Env trimer, BG505 SOSIP.664 gp140, expresses multiple epitopes for broadly neutralizing but not non-neutralizing antibodies. *PLoS Pathog.* 9: e1003618.

18. Cheng, C., M. Pancera, A. Bossert, S. D. Schmidt, R. E. Chen, X. Chen, A. Druz, S. Narpala, N. A. Doria-Rose, A. B. McDermott, et al. 2015. Immunogenicity of a prefusion HIV-1 envelope trimer in complex with a quaternary-structure-specific antibody. *J. Virol.* 90: 2740–2755.

19. de Taeye, S. W., G. Ozorowski, A. Torrents de la Peña, M. Guttman, J. P. Julien, T. L. van den Kerkhof, J. A. Burger, L. K. Pritchard, P. Pugach, A. Yasmeen, et al. 2015. Immunogenicity of stabilized HIV-1 envelope trimers with reduced exposure of non-neutralizing epitopes. *Cell* 163: 1702–1715.

20. Sanders, R. W., M. J. van Gils, R. Derking, D. Sok, T. J. Ketas, J. A. Burger, G. Ozorowski, A. Cupo, C. Simonich, L. Goo, et al. 2015. HIV-1 VACCINES. HIV-1 neutralizing antibodies induced by native-like envelope trimers. *Science* 349: aac4223.

21. Douagi, I., M. N. Forsell, C. Sundling, S. O'Dell, Y. Feng, P. Dosenovic, Y. Li, R. Seder, L. Loré, J. R. Mascola, et al. 2010. Influence of novel CD4 binding-defective HIV-1 envelope glycoprotein immunogens on neutralizing antibody and T-cell responses in nonhuman primates. *J. Virol.* 84: 1683–1695.

22. Feng, Y., K. McKee, K. Tran, S. O'Dell, S. D. Schmidt, A. Phogat, M. N. Forsell, G. B. Karlsson Hedestam, J. R. Mascola, and R. T. Wyatt. 2012. Biochemically defined HIV-1 envelope glycoprotein variant immunogens display differential binding and neutralizing specificities to the CD4-binding site. *J. Biol. Chem.* 287: 5673–5686.

23. Mörner, A., I. Douagi, M. N. Forsell, C. Sundling, P. Dosenovic, S. O'Dell, B. Dey, P. D. Kwong, G. Voss, R. Thorstensson, et al. 2009. Human immunodeficiency virus type 1 env trimer immunization of macaques and impact of priming with viral vector or stabilized core protein. *J. Virol.* 83: 540–551.

24. Sundling, C., Y. Li, N. Huynh, C. Poulsen, R. Wilson, S. O'Dell, Y. Feng, J. R. Mascola, R. T. Wyatt, and G. B. Karlsson Hedestam. 2012. High-resolution definition of vaccine-elicited B cell responses against the HIV primary receptor binding site. *Sci. Transl. Med.* 4: 142ra96.

25. Posner, M. R., L. A. Cavacini, C. L. Emes, J. Power, and R. Byrn. 1993. Neutralization of HIV-1 by F105, a human monoclonal antibody to the CD4 binding site of gp120. *J. Acquir. Immune Defic. Syndr.* 6: 7–14.

26. Zhou, T., N. A. Doria-Rose, C. Cheng, G. B. E. Stewart-Jones, G. Y. Chuang, M. Chambers, A. Druz, H. Geng, K. McKee, Y. D. Kwon, et al. 2017. Quantification of the impact of the HIV-1-glycan shield on antibody elicitation. *Cell Rep.* 19: 719–732.

27. Stewart-Jones, G. B., C. Soto, T. Lemmin, G. Y. Chuang, A. Druz, R. Kong, P. V. Thomas, K. Wagh, T. Zhou, A. J. Behrens, et al. 2016. Trimeric HIV-1-Env structures define glycan shields from clades A, B, and G. *Cell* 165: 813–826.

28. Jardine, J., J. P. Julien, S. Menis, T. Ota, O. Kalyuzhniy, A. McGuire, D. Sok, P. S. Huang, S. MacPherson, M. Jones, et al. 2013. Rational HIV immunogen design to target specific germline B cell receptors. *Science* 340: 711–716.

29. McGuire, A. T., S. Hoot, A. M. Dreyer, A. Lippy, A. Stuart, K. W. Cohen, J. Jardine, S. Menis, J. F. Scheid, A. P. West, et al. 2013. Engineering HIV envelope protein to activate germline B cell receptors of broadly neutralizing anti-CD4 binding site antibodies. *J. Exp. Med.* 210: 655–663.

30. Jardine, J. G., D. W. Kulp, C. Havenar-Daughton, A. Sarkar, B. Briney, D. Sok, F. Sesterhenn, J. Ereño-Orbea, O. Kalyuzhniy, I. Deresa, et al. 2016. HIV-1 broadly neutralizing antibody precursor B cells revealed by germline-targeting immunogen. *Science* 351: 1458–1463.

31. Havenar-Daughton, C., A. Sarkar, D. W. Kulp, L. Toy, X. Hu, I. Deresa, O. Kalyuzhniy, K. Kaushik, A. A. Upadhyay, S. Menis, et al. 2018. The human naive B cell repertoire contains distinct subclasses for a germline-targeting HIV vaccine immunogen. *Sci. Transl. Med.* 10: eaat0381.

32. Havenar-Daughton, C., J. H. Lee, and S. Crotty. 2017. Tfh cells and HIV bnAbs, an immunodominance model of the HIV neutralizing antibody generation problem. *Immunol. Rev.* 275: 49–61.

33. Navis, M., K. Tran, S. Bale, J. Guenaga, R. Wilson, M. Soldemo, K. McKee, C. Sundling, J. Mascola, et al. 2014. HIV-1 receptor binding site-directed antibodies using a VH1-2 gene segment orthologue are activated by Env trimer immunization. *PLoS Pathog.* 10: e1004337.

34. Li, Y., S. O'Dell, L. M. Walker, X. Wu, J. Guenaga, Y. Feng, S. D. Schmidt, K. McKee, M. K. Louder, J. E. Ledgerwood, et al. 2011. Mechanism of neutralization by the broadly neutralizing HIV-1 monoclonal antibody VRC01. *J. Virol.* 85: 8954–8967.

35. Li, Y., S. O'Dell, R. Wilson, X. Wu, S. D. Schmidt, C. M. Hogerkorp, M. K. Louder, N. S. Longo, C. Poulsen, J. Guenaga, et al. 2012. HIV-1 neutralizing

antibodies display dual recognition of the primary and coreceptor binding sites and preferential binding to fully cleaved envelope glycoproteins. *J. Virol.* 86: 11231–11241.

36. Zhou, T., I. Georgiev, X. Wu, Z. Y. Yang, K. Dai, A. Finzi, Y. D. Kwon, J. F. Scheid, W. Shi, L. Xu, et al. 2010. Structural basis for broad and potent neutralization of HIV-1 by antibody VRC01. *Science* 329: 811–817.

37. Chen, L., Y. D. Kwon, T. Zhou, X. Wu, S. O'Dell, L. Cavacini, A. J. Hessell, M. Pancera, M. Tang, L. Xu, et al. 2009. Structural basis of immune evasion at the site of CD4 attachment on HIV-1 gp120. *Science* 326: 1123–1127.

38. Chen, Y., R. Wilson, S. O'Dell, J. Guenaga, Y. Feng, K. Tran, C. I. Chiang, H. E. Arendt, J. DeStefano, J. R. Mascola, et al. 2016. An HIV-1 Env-antibody complex focuses antibody responses to conserved neutralizing epitopes. *J. Immunol.* 197: 3982–3998.

39. Pancera, M., S. Majeed, Y. E. Ban, L. Chen, C. C. Huang, L. Kong, Y. D. Kwon, J. Stuckey, T. Zhou, J. E. Robinson, et al. 2010. Structure of HIV-1 gp120 with gp41-interactive region reveals layered envelope architecture and basis of conformational mobility. *Proc. Natl. Acad. Sci. USA* 107: 1166–1171.

40. Tolbert, W. D., N. Gohain, N. Alsahafi, V. Van, C. Orlandi, S. Ding, L. Martin, A. Finzi, G. K. Lewis, K. Ray, and M. Pazgier. 2017. Targeting the late stage of HIV-1 entry for antibody-dependent cellular cytotoxicity: structural basis for Env epitopes in the C11 region. *Structure* 25: 1719–1731.e4.

41. Moore, J. P., and J. Sodroski. 1996. Antibody cross-competition analysis of the human immunodeficiency virus type 1 gp120 exterior envelope glycoprotein. *J. Virol.* 70: 1863–1872.

42. Kwon, Y. D., A. Finzi, X. Wu, C. Dogo-Isonagie, L. K. Lee, L. R. Moore, S. D. Schmidt, J. Stuckey, Y. Yang, T. Zhou, et al. 2012. Unliganded HIV-1 gp120 core structures assume the CD4-bound conformation with regulation by quaternary interactions and variable loops. *Proc. Natl. Acad. Sci. USA* 109: 5663–5668.

43. Comeau, S. R., D. W. Gatchell, S. Vajda, and C. J. Camacho. 2004. ClusPro: an automated docking and discrimination method for the prediction of protein complexes. *Bioinformatics* 20: 45–50.

44. Guan, Y., M. Pazgier, M. M. Sajadi, R. Kamin-Lewis, S. Al-Darmarki, R. Flinko, E. Lovo, X. Wu, J. E. Robinson, M. S. Seaman, et al. 2013. Diverse specificity and effector function among human antibodies to HIV-1 envelope glycoprotein epitopes exposed by CD4 binding. *Proc. Natl. Acad. Sci. USA* 110: E69–E78.

45. Lyskov, S., F. C. Chou, S. O. Conchúir, B. S. Der, K. Drew, D. Kuroda, J. Xu, B. D. Weitzner, D. P. Renfrew, P. Sripakdeevong, et al. 2013. Serverification of molecular modeling applications: the Rosetta Online Server that Includes Everyone (ROSIE). *PLoS One* 8: e63906.

46. Pettersen, E. F., T. D. Goddard, C. C. Huang, G. S. Couch, D. M. Greenblatt, E. C. Meng, and T. E. Ferrin. 2004. UCSF Chimera--a visualization system for exploratory research and analysis. *J. Comput. Chem.* 25: 1605–1612.

47. Fiser, A., and A. Sali. 2003. Modeller: generation and refinement of homology-based protein structure models. *Methods Enzymol.* 374: 461–491.

48. Guenaga, J., V. Dubrovskaya, N. de Val, S. K. Sharma, B. Carrette, A. B. Ward, and R. T. Wyatt. 2015. Structure-guided redesign increases the propensity of HIV env to generate highly stable soluble trimers. *J. Virol.* 90: 2806–2817.

49. Dubrovskaya, V., J. Guenaga, N. de Val, R. Wilson, Y. Feng, A. Movsesyan, G. B. Karlsson Hedestam, A. B. Ward, and R. T. Wyatt. 2017. Targeted N-glycan deletion at the receptor-binding site retains HIV Env NFL trimer integrity and accelerates the elicited antibody response. *PLoS Pathog.* 13: e1006614.

50. Soldemo, M., G. K. Pedersen, and G. B. Karlsson Hedestam. 2014. HIV-1 Env-specific memory and germinal center B cells in C57BL/6 mice. *Viruses* 6: 3400–3414.

51. Hu, J. K., J. C. Crampton, A. Cupo, T. Ketas, M. J. van Gils, K. Sliepen, S. W. de Taeye, D. Sok, G. Ozorowski, I. Deresa, et al. 2015. Murine antibody responses to cleaved soluble HIV-1 envelope trimers are highly restricted in specificity. *J. Virol.* 89: 10383–10398.

52. Wang, Y., C. Sundling, R. Wilson, S. O'Dell, Y. Chen, K. Dai, G. E. Phad, J. Zhu, Y. Xiao, J. R. Mascola, et al. 2016. High-resolution longitudinal study of HIV-1 env vaccine-elicited B cell responses to the virus primary receptor binding site reveals affinity maturation and clonal persistence. *J. Immunol.* 196: 3729–3743.

53. Tiller, T., C. E. Busse, and H. Wardemann. 2009. Cloning and expression of murine Ig genes from single B cells. *J. Immunol. Methods* 350: 183–193.

54. Alamyar, E., P. Duroux, M. P. Lefranc, and V. Giudicelli. 2012. IMGT(®) tools for the nucleotide analysis of immunoglobulin (IG) and T cell receptor (TR) V-(D)-J repertoires, polymorphisms, and IG mutations: IMGT/V-QUEST and IMGT/HighV-QUEST for NGS. *Methods Mol. Biol.* 882: 569–604.

55. Tran, K., C. Poulsen, J. Guenaga, N. de Val, R. Wilson, C. Sundling, Y. Li, R. L. Stanfield, I. A. Wilson, A. B. Ward, et al. 2014. Vaccine-elicited primate antibodies use a distinct approach to the HIV-1 primary receptor binding site informing vaccine redesign. [Published erratum appears in 2014 *Proc. Natl. Acad. Sci. USA* 111: 1403776111.] *Proc. Natl. Acad. Sci. USA* 111: E738–E747.

56. Li, M., F. Gao, J. R. Mascola, L. Stamatatos, V. R. Polonis, M. Koutsoukos, G. Voss, P. Goepfert, P. Gilbert, K. M. Greene, et al. 2005. Human immunodeficiency virus type 1 env clones from acute and early subtype B infections for standardized assessments of vaccine-elicited neutralizing antibodies. *J. Virol.* 79: 10108–10125.

57. Wu, X., T. Zhou, S. O'Dell, R. T. Wyatt, P. D. Kwong, and J. R. Mascola. 2009. Mechanism of human immunodeficiency virus type 1 resistance to monoclonal antibody B12 that effectively targets the site of CD4 attachment. *J. Virol.* 83: 10892–10907.

58. Seaman, M. S., H. Janes, N. Hawkins, L. E. Grandpre, C. Devoy, A. Giri, R. T. Coffey, L. Harris, B. Wood, M. G. Daniels, et al. 2010. Tiered categorization of a diverse panel of HIV-1 Env pseudoviruses for assessment of neutralizing antibodies. *J. Virol.* 84: 1439–1452.

59. Schneidman-Duhovny, D., M. Hammel, J. A. Tainer, and A. Sali. 2016. FoXS, FoXSDock and MultiFoXS: single-state and multi-state structural modeling of proteins and their complexes based on SAXS profiles. *Nucleic Acids Res.* 44(W1): W424–W429.

60. Franke, D., M. V. Petoukhov, P. V. Konarev, A. Panjkovich, A. Tuukkanen, H. D. T. Mertens, A. G. Kikhney, N. R. Hajizadeh, J. M. Franklin, C. M. Jeffries, and D. I. Svergun. 2017. *ATSAS 2.8*: a comprehensive data analysis suite for small-angle scattering from macromolecular solutions. *J. Appl. Cryst.* 50: 1212–1225.

61. Svergun, D. I. 1999. Restoring low resolution structure of biological macromolecules from solution scattering using simulated annealing. *Biophys. J.* 76: 2879–2886.

62. Kong, L., B. Ju, Y. Chen, L. He, L. Ren, J. Liu, K. Hong, B. Su, Z. Wang, G. Ozorowski, et al. 2016. Key gp120 glycans pose roadblocks to the rapid development of VRC01-class antibodies in an HIV-1-infected Chinese donor. *Immunity* 44: 939–950.

63. Dey, B., K. Svehla, L. Xu, D. Wycuff, T. Zhou, G. Voss, A. Phogat, B. K. Chakrabarti, Y. Li, G. Shaw, et al. 2009. Structure-based stabilization of HIV-1 gp120 enhances humoral immune responses to the induced co-receptor binding site. *PLoS Pathog.* 5: e1000445.

64. Ahmad, Z. A., S. K. Yeap, A. M. Ali, W. Y. Ho, N. B. Alitheen, and M. Hamid. 2012. scFv antibody: principles and clinical application. *Clin. Dev. Immunol.* 2012: 980250.

65. Kriangkum, J., B. Xu, L. P. Nagata, R. E. Fulton, and M. R. Suresh. 2001. Bispecific and bifunctional single chain recombinant antibodies. *Biomol. Eng.* 18: 31–40.

66. Briney, B., D. Sok, J. G. Jardine, D. W. Kulp, P. Skog, S. Menis, R. Jacak, O. Kalyuzhniy, N. de Val, F. Sesterhenn, et al. 2016. Tailored immunogens direct affinity maturation toward HIV neutralizing antibodies. *Cell* 166: 1459–1470.e11.

67. Acharya, P., W. D. Tolbert, N. Gohain, X. Wu, L. Yu, T. Liu, W. Huang, C. C. Huang, Y. D. Kwon, R. K. Louder, et al. 2014. Structural definition of an antibody-dependent cellular cytotoxicity response implicated in reduced risk for HIV-1 infection. *J. Virol.* 88: 12895–12906.

68. Derking, R., G. Ozorowski, K. Sliepen, A. Yasmeen, A. Cupo, J. L. Torres, J. P. Julien, J. H. Lee, T. van Montfort, S. W. de Taeye, et al. 2015. Comprehensive antigenic map of a cleaved soluble HIV-1 envelope trimer. *PLoS Pathog.* 11: e1004767.

69. Shi, B., L. Ma, X. He, X. Wang, P. Wang, L. Zhou, and X. Yao. 2014. Comparative analysis of human and mouse immunoglobulin variable heavy regions from IMGT/LIGM-DB with IMGT/HighV-QUEST. *Theor. Biol. Med. Model.* 11: 30.

70. Jardine, J. G., T. Ota, D. Sok, M. Pauthner, D. W. Kulp, O. Kalyuzhniy, P. D. Skog, T. C. Thinnes, D. Bhullar, B. Briney, et al. 2015. HIV-1 VACCINES. Priming a broadly neutralizing antibody response to HIV-1 using a germline-targeting immunogen. *Science* 349: 156–161.

71. Abbott, R. K., J. H. Lee, S. Menis, P. Skog, M. Rossi, T. Ota, D. W. Kulp, D. Bhullar, O. Kalyuzhniy, C. Havenar-Daughton, et al. 2018. Precursor frequency and affinity determine B cell competitive fitness in germinal centers, tested with germline-targeting HIV vaccine immunogens. *Immunity* 48: 133–146.e6.

72. West, A. P., Jr., R. Diskin, M. C. Nussenzweig, and P. J. Bjorkman. 2012. Structural basis for germ-line gene usage of a potent class of antibodies targeting the CD4-binding site of HIV-1 gp120. *Proc. Natl. Acad. Sci. USA* 109: E2083–E2090.

73. Escolano, A., J. M. Steichen, P. Dosenovic, D. W. Kulp, J. Golijanin, D. Sok, N. T. Freund, A. D. Gitlin, T. Oliveira, T. Araki, et al. 2016. Sequential immunization elicits broadly neutralizing anti-HIV-1 antibodies in Ig knockin mice. *Cell* 166: 1445–1458.e12.

74. Klasse, P. J., C. C. LaBranche, T. J. Ketas, G. Ozorowski, A. Cupo, P. Pugach, R. P. Ringe, M. Golabek, M. J. van Gils, M. Guttman, et al. 2016. Sequential and simultaneous immunization of rabbits with HIV-1 envelope glycoprotein SOSIP.664 trimers from clades A, B and C. *PLoS Pathog.* 12: e1005864.

75. Wang, S. 2017. Optimal sequential immunization can focus antibody responses against diversity loss and distraction. *PLoS Comput. Biol.* 13: e1005336.

76. Steichen, J. M., D. W. Kulp, T. Tokatlian, A. Escolano, P. Dosenovic, R. L. Stanfield, L. E. McCoy, G. Ozorowski, X. Hu, O. Kalyuzhniy, et al. 2016. HIV vaccine design to target germline precursors of glycan-dependent broadly neutralizing antibodies. *Immunity* 45: 483–496.

77. Tian, M., C. Cheng, X. Chen, H. Duan, H. L. Cheng, M. Dao, Z. Sheng, M. Kimble, L. Wang, S. Lin, et al. 2016. Induction of HIV neutralizing antibody lineages in mice with diverse precursor repertoires. *Cell* 166: 1471–1484.e18.

78. Dosenovic, P., L. von Boehmer, A. Escolano, J. Jardine, N. T. Freund, A. D. Gitlin, A. T. McGuire, D. W. Kulp, T. Oliveira, L. Scharf, et al. 2015. Immunization for HIV-1 broadly neutralizing antibodies in human Ig knockin mice. *Cell* 161: 1505–1515.

79. McGuire, A. T., M. D. Gray, P. Dosenovic, A. D. Gitlin, N. T. Freund, J. Petersen, C. Correnti, W. Johnsen, R. Kegel, A. B. Stuart, et al. 2016. Specifically modified Env immunogens activate B-cell precursors of broadly neutralizing HIV-1 antibodies in transgenic mice. *Nat. Commun.* 7: 10618.

80. Whitaker, N., J. M. Hickey, K. Kaur, J. Xiong, N. Sawant, A. Cupo, W. H. Lee, G. Ozorowski, M. Medina-Ramírez, A. B. Ward, et al. 2019. Developability assessment of physicochemical properties and stability profiles of HIV-1 BG505 SOSIP.664 and BG505 SOSIP.v4.1-GT1.1 gp140 envelope glycoprotein trimers as candidate vaccine antigens. *J. Pharm. Sci.* 108: 2264–2277.

81. Medina-Ramírez, M., F. Garces, A. Escolano, P. Skog, S. W. de Taeye, I. Del Moral-Sanchez, A. T. McGuire, A. Yasmeen, A. J. Behrens, G. Ozorowski, et al. 2017. Design and crystal structure of a native-like HIV-1 envelope trimer that engages multiple broadly neutralizing antibody precursors in vivo. *J. Exp. Med.* 214: 2573–2590.

82. McGuire, A. T., A. M. Dreyer, S. Carbonetti, A. Lippy, J. Glenn, J. F. Scheid, H. Mouquet, and L. Stamatatos. 2014. HIV antibodies. Antigen modification regulates competition of broad and narrow neutralizing HIV antibodies. *Science* 346: 1380–1383.